ELSEVIER

Chemical Engineering Journal 115 (2006) 173–193

Chemical Engineering Journal

www.elsevier.com/locate/cej

Effect of impeller design on the flow pattern and mixing in stirred tanks

T. Kumaresan, Jyeshtharaj B. Joshi *

Institute of Chemical Technology, University of Mumbai, Matunga, Mumabi 400019, India

Received 14 April 2005; received in revised form 7 October 2005; accepted 7 October 2005

Abstract

The flow pattern and power number in a vessel depend on the impeller blade angle, number of blades, blade width, blade twist, blade thickness, pumping direction and interaction of flow with the vessel wall. Measurements of the power consumption and flow pattern have been carried out in a stirred vessel of 0.5 m diameter for the range of impellers to study the effect of blade shape on the flow pattern. The comparison of the flow pattern (average velocity, turbulent kinetic energy, maximum energy dissipation rate, average shear rate and turbulent normal stress) has been presented on the basis of equal power consumption to characterize the flow generated by different impeller geometries. Comparisons of LDA measurements and CFD predictions have been presented. The good comparison indicates the validity of the CFD model.

Keywords: Stirred vessel; Impeller design; Impeller types; Mixing; CFD; Sliding mesh; Fluid mechanics

1. Introduction

Stirred vessels are widely used in chemical, pharmaceutical, food and metallurgical process industries as well in municipal and industrial wastewater treatment. In these processes, the requirement of quality of mixing varies over a wide range. These include blending of low viscosity of liquids, high viscosity liquids or high viscosity liquids with low viscosity liquids and vice versa, solid-solid mixing, etc. These also include heat transfer and large number of dispersion applications such as solid–liquid, gas–liquid, liquid–liquid, gas–liquid–solid, gas–liquid–liquid–solid, etc. The quality of mixing mainly depends upon the relative distribution of mean and turbulent kinetic energy. One extreme is the absence of turbulence and the entire energy exists in the form of mean kinetic energy. The other extreme is that the flow is turbulent at all the locations and the mean velocities are zero. Obviously, the real flow is in between the two extremes and depends upon impeller design, diameter and the location of impeller/s, vessel diameter, bottom design and internals such as coils, baffles, draft tube, etc. The desired flow pattern (relative distribution of mean and turbulent kinetic energy) depends upon the application. For instance, blending application prefers all the energy in the form of mean and minimal turbulent kinetic energy (even <5% [1]). On contrast, colloidal mills, homogenizers and emulsifiers need highly turbulent flows. All the other applications can be conveniently classified according to their need of energy distribution.

In stirred vessels, the quality of flow generated by the impeller mainly depends upon the impeller design. Typically, low power number (0.1–0.5) impellers generate mean flow whereas high power number impellers (>3) generate flow having more turbulent kinetic energy. As the flow proceeds from the impeller and circulates within the vessel, the mean kinetic energy is converted into turbulent kinetic energy and as mentioned earlier, the relative distribution at any location depends upon the design of the impeller, vessel and internals. In view of such an immense importance of the knowledge of quality of flow, vigorous research efforts have been made during the last 50 years using various flow measurement techniques and computational fluid dynamics (CFD). A brief review has been presented below for getting a flavour of the existing status of knowledge.

The on going demand for the improved impeller designs usually comes from the users of industrial mixing equipment when the vessels are to be designed for new plants or improvement in the existing design is desired for enhancing quality, capacity, process efficiency and energy efficiency. For meeting these objectives, it is imperative that the relationship between the flow pattern and the design objective is understood. One of the flow characteristics affecting the impeller flow efficiency is the presence of trailing vortices generated at the tip of the

* Corresponding author. Tel.: +91 22 414 5616; fax: +91 22 414 5614.
E-mail address: jbj@udct.org (J.B. Joshi).

1385-8947/$ – see front matter © 2005 Elsevier B.V. All rights reserved.
doi:10.1016/j.cej.2005.10.002

Nomenclature

B_C	baffle clearance (m)
B_{tk}	impeller blade thickness (m)
B_T	baffle thickness (m)
B_W	baffle width (m)
c	concentration in the cell (kmol m^{-3})
C	clearance between the impeller to the vessel base (m)
CMC	carboxy methyl cellulose
C_μ, $C_{\varepsilon 1}$, $C_{\varepsilon 2}$	k–ε model constant
D	impeller diameter (m)
D_h	diameter of the impeller hub (m)
H	liquid height (m)
k	local turbulent kinetic energy (m^2 s^{-2})
k_{avg}	average turbulent kinetic energy (m^2 s^{-2})
L	length of the blade from the hub to periphery (m)
LDA	laser Doppler anemometer
N	impeller rotational speed (s^{-1})
N_b	number of baffles
$N_{P,exp}$	experimental power number ($P/\rho N^3 D^5$)
$N_{P,Pred}$	predicted power number, Eq. (4)
N_{QP}	primary flow number, Eq. (1)
N_{QS}	secondary flow number, Eq. (2)
N_{Re}	Reynolds number (ND^2/γ)
P	power consumption (w)
PBTD	pitched blade turbine downflow
PBTU	pitched blade turbine upflow
r	radial coordinate (m)
R	vessel radius (m)
RPS	revolutions per second
R_I	radial location till impeller periphery (m)
R_R	radial location till reversal axial flow (m)
S_Φ	source term for generalized flow variable Φ
T	tank diameter (m)
v_r, v_z, v_θ	mean velocity in the radial, axial and tangential direction respectively (m s^{-1})
v'_r, v'_z, v'_θ	fluctuating velocity in the radial, axial and tangential direction respectively (m s^{-1})
V	operating volume (m^3)
U_{tip}	impeller tip velocity (m s^{-1})
w_g	weight exerted (kg)
W	impeller blade width (m)
W_h	impeller blade width near the hub (m)
W_t	impeller blade width at the blade tip (m)
z	axial coordinate (m)

Superscript

S	small impeller diameter ($D/T = 0.2$)

Greek symbols

γ	kinematic viscosity (m^2 s^{-1})
γ_{avg}	average shear rate (s^{-1})
γ_{zr}, $\gamma_{r\theta}$, $\gamma_{\theta z}$	shear components in z–r, r–θ and θ–z direction (s^{-1})
Γ	effective diffusivity consisting of molecular plus turbulent diffusivity (m^2 s^{-1})
ε	energy dissipated per unit mass (m^2 s^{-3})
$\overline{\varepsilon}$	average energy dissipated per unit mass (m^2 s^{-3})
ε_{max}	maximum energy dissipated below the impeller (m^2 s^{-3})
θ	tangential coordinate
θ_{CFD}	predicted mixing time (s)
θ_{exp}	experimental mixing time (s)
ν_t	kinematic viscosity (m^2 s^{-1})
ρ	density (kg m^{-3})
$\overline{\tau}_N$	average turbulent normal stress (N m^{-2})
τ_0	torque (kg m^2 s^{-2})
σ_ε, σ_k	k–ε model constant
Φ	generalized flow variable

impeller blades. Firoz et al. [2] studied the strength of the trailing vortex structures close to the four-bladed 45° pitched blade turbine using vorticity maps. It is possible to minimize the vortex size and improve the axial flow efficiency of such impellers by proper designing of the blade tip shape. However, more details of trailing vortices structures for four bladed pitched blade turbine are given by Schafer et al. [3]. Fasano et al. [4] indicated that the large trailing vortex in four-bladed 45° pitched blade turbine (mixed flow impeller) accounts for its lower efficiency compared to that of three-bladed Chemineer HE-3 impeller. Further, they found that the three-bladed HE-3 impeller provides a more stable heat transfer profile at the vessel wall than that of the four-bladed PBTD impeller. The overall heat transfer coefficient in the stirred vessel with HE-3 impeller was found to be 10% higher than that of mixed flow impeller.

Ranade and Joshi [5] investigated the effect of impeller blade pitch (30°, 45° and 60°) on the flow pattern and established that an impeller blade angle in pitched blade turbine significantly affects the flow characteristics. However, the blade width was found important for radial flow disc turbines especially in the gas–liquid dispersion operation. We-Ming et al. [6] investigated the role of blade width on the generated vortex structure at impeller blade tip using a single disc turbine at equal power input. They observed that the impeller with larger blade ($W/D = 0.19$) produces a fully developed vortex flow and the smaller blade impeller ($W/D = 0.07$) produces a stronger shear stress due to the mergence of the two symmetric vortices. Rutherford et al. [7] and Bujalski et al. [8] observed the importance of blade thickness for disc turbine where the maximum mean velocity in the impeller discharge region was reduced approximately to $0.18U_{tip}$ when B_{tk}/D was increased from 0.0082 to 0.0337. Medek and Fort [9]. Fentiman et al. [10] made a slight blade twist in the three bladed hydrofoil impeller and found that mixing efficiency increased with the change in blade twist. However, more number of hydrofoil impellers must be investigated to find the effect of mixing efficiency on the bladed twist.

Jaworski et al. [11] compared the superiority of commercial hydrofoils (Chemineer HE-3 and Prochem Maxflo T) in

generating the circulating flow at equal power input. Although the observed trends in the mean axial and radial flows are similar, there was a drastic change in their level of magnitudes. Both the primary flow number (N_{QP}) and secondary flow number (N_{QS}) of broad bladed hydrofoil (Prochem Maxflo T) was 50% greater than that of the narrow bladed hydrofoil (Chemineer HE-3). Further, they have proposed that the net circulation produced by an impeller is more important than the pumping capacity. Tomas et al. [12] experimented commercial techmix 335-hydrofoil impeller on the mixing intensity of dispersion. They observed that the impellers with lower power number (less than unity) provide higher dispersion mixing intensities, while the impellers with higher power number gave better mass transfer performance. Patwardhan and Joshi [1] pointed out that mixing time was well correlated with N_{QS} rather than N_{QP} that implies that the circulation time preferably should be calculated with the total flow (primary + entrained) of an impeller, which emphasizes the importance of entrained flow.

Bugay et al. [13] performed experiments on the Lightnin A310 impeller ($N_{QP} = 0.55$) focusing on the mean flow and turbulent kinetic energy using PIV. They have observed that the magnitude of maximum axial velocity was found to be 30% of the impeller tip speed (U_{tip}) at $r/R = 0.6$. Also, they have observed that the liquid at free surface rotates in the same direction as the impeller, in the vessel core region ($r/R < 0.5$) and the liquid rotation was opposite close to the vessel wall ($r/R > 0.5$). However, in order to further improve the mixing efficiency of such impellers, the hydrodynamics of more number of broad bladed hydrofoils with modified blade design has to be investigated. Mavros et al. [14] compared the flow efficiency of three commercially available impellers (Rushton turbine, Mixel TT and Lightnin A310) using LDA. The Mixel TT was found to have the high flow efficiency of 70.9% whereas Rushton turbine and Lightnin A310 had flow efficiency of only 52.7% and 46.2%, respectively. Further studies on those three impellers using viscous fluid (1% CMC solution) gave less than 26% hydraulic efficiency. Zhou and Kresta [15] concentrated on the turbulent kinetic energy induced by three different impellers (Rushton turbine, four-bladed PBTD and Lightnin A310) in the impeller discharge region using LDA. They observed that the fluctuations in the direction of the principal flow of an impeller contributes more towards the turbulent kinetic energy i.e., radial fluctuations for Rushton turbine and axial fluctuations for PBTD and A310. In order to pursue with such an assumption of local isotropy ($3u'^2_z/2$), experiments on more number of impeller blade designs must be considered to quantify the exact level of participation of the principal fluctuation on the turbulent kinetic energy budget.

Patwardhan and Joshi [1] have indicated an enormous scope for improvement in the mixing efficiency (mixing time per unit power consumption) by achieving desired combination of mean and turbulence at various locations in the tank. In view of this, it was thought desirable to undertake a systematic investigation of the effect of various impeller designs on the flow pattern and mixing time. In the present work, the investigation has been focused on axial flow impellers.

2. Experimental methods and impeller nomenclature

Experiments were performed in 500 mm i.d. flat bottom transparent (Perspex) cylindrical vessel. The baffle width ($B_W = T/10$), baffle thickness ($B_T = 4.5$ mm) and the clear liquid height, $H = T$ were maintained constant for all the configurations used in this work. Tap water was used as the working fluid. A two HP variable speed motor supplied the necessary power to the system that enabled the shaft to rotate in the range 0.167–20 revolutions per second. In all the cases the impeller speed was maintained in such a way that there was no air entrapment from the liquid surface.

Experiments have been performed using pitched blade turbines with various blade designs. The impeller nomenclature is as follows:

(i) The four letters (PBTD) in the impeller nomenclature stands for pitched blade turbine downflow whereas PBTU stands for pitched blade turbine upflow and the two-digit number following immediately is the blade angle in degrees (°) at impeller hub.
(ii) The consequent two-digit number represents the blade angle at the impeller blade tip. The difference in these angles gives the blade twist, representing the presence of blade twist in the impeller. If the blade angle only near the impeller hub is given without the blade tip angle, it means the blades are straight without blade twists.
(iii) The letter 'W' following the blade tip angle represents the blade width and a consequent two-digit number represents blade width in mm at the impeller hub and the successive two-digit stands for the blade width at impeller blade tip. If the blade width only near the impeller hub is given without the blade width at impeller periphery, it represents the presence of constant blade width.
(iv) Finally, a single digit number that is followed after a dash sign stands for the number of blades fixed to the impeller hub.

Hydrofoil impellers are increasingly becoming popular. It is claimed that these impellers have superior characteristics as compared to the standard impeller designs. Hence, the flow patterns of six narrow bladed hydrofoils and four broad bladed hydrofoils have also been performed in this study. A similar nomenclature is followed for the narrow bladed hydrofoils as pitched blade turbines. All narrow bladed hydrofoils used in this work are three-bladed.

The nomenclature for broad bladed hydrofoils that are of high solidity ratios is as follows. The blades of the three-bladed HF2 impeller were convex in shape and the curvature is widthwise. The radius of curvature is approximately 100 mm. The HF3 impeller was similar in shape to HF2 impeller, but it has four blades with radius of curvature approximately 110 mm. The blade curvature for HF3045-4 and HF4560-4 is very similar to that of HF3 hydrofoil with blade twist of 15°. Photographic views of all the impellers investigated are given in Fig. 1. The flow measurements were done in the mid-baffle plane where an

input power level of 1 W/kg and impeller off bottom clearance of $C/T = 0.33$ were maintained for all impellers studied. However, the power measurements were compared at three different impeller off bottom clearances of $C/T = 0.25$, 0.33 and 0.5.

2.1. Power number measurements

The power consumption in an impeller agitated vessel was calculated using the load (w_g) measured by the load cell setup associated with the torque table with the controlled traversing mechanism [16]. The position of the shaft was fixed while the impeller off-bottom clearance could be altered by changing the vessel position by vertically traversing the torque table. The load cell was calibrated each time before the measurements were carried out. Statistically sufficient (10–12) readings were taken for each setup to yield meaningful average load that was used for computing the power consumption, which in turn was used for the estimation of power number (N_P).

2.2. Mixing time measurements

The mixing time was measured using four conductivity probes located at various positions so as represent all the regions of the stirred vessel. Probe 1 was located 50 mm below the water level and 20° ahead to the baffle. Probe 2 was located 110 mm below the water level and midway between the two baffles. Probe 3 was located 340 mm below the water surface and midway between the baffles (in the impeller plane). Probe 4 was located 20 mm above the vessel base and 40 mm behind the baffle. Sodium chloride solution (2 M) was used as a tracer. An impulse input of tracer (volume = 0.1 L) was injected on the liquid surface in the midway between the baffles and 100 mm away from the shaft. Data acquisition was continued for sufficiently longer time so as to allow for closer approach to the steady state in the concentration profiles. The mixing time was estimated for each of the probes as the time required to attain the final concentration within ±2% of the average concentration. Final mixing time was obtained as the average of all the mixing times indicated by four probes.

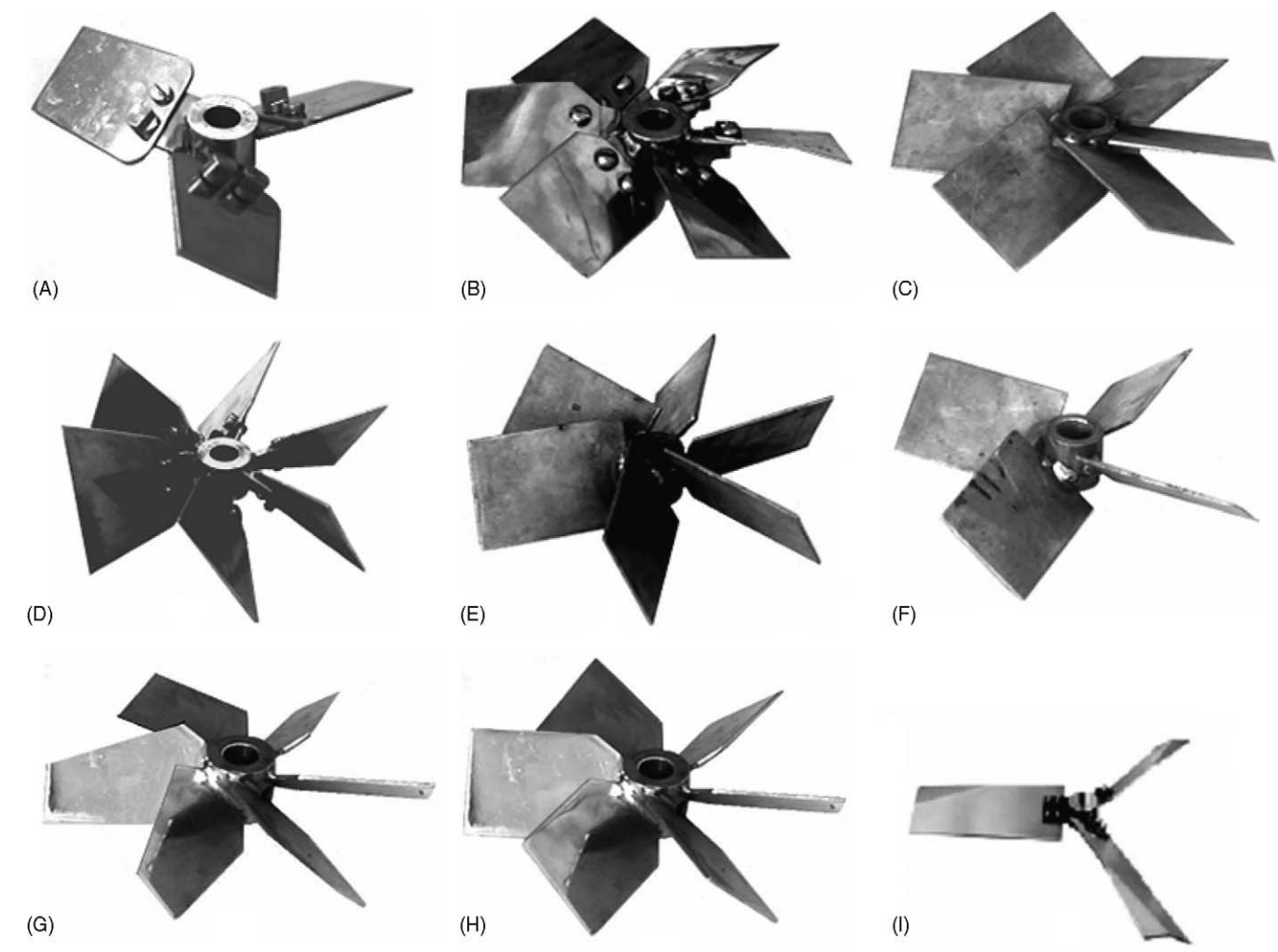

Fig. 1. Impeller designs. (A) PBTD30W5545-3; (B) PBTD3020W50-6; (C) PBTD30W50-6; (D) PBTD60W3085-6; (E) PBTD60W50-6; (F) PBTD45W50-4; (G) PBTD45W5030-6; (H) PBTD45W3050-6; (I) HF30W25-3; (J) HF45W25-3; (K) HF4530W2517-3; (L) HF6030W2513-3; (M) HF6045W2520-3; (N) HF2; (O) HF3; (P) HF3060-4; (Q) HF4560-4; (R) standard disc turbine.

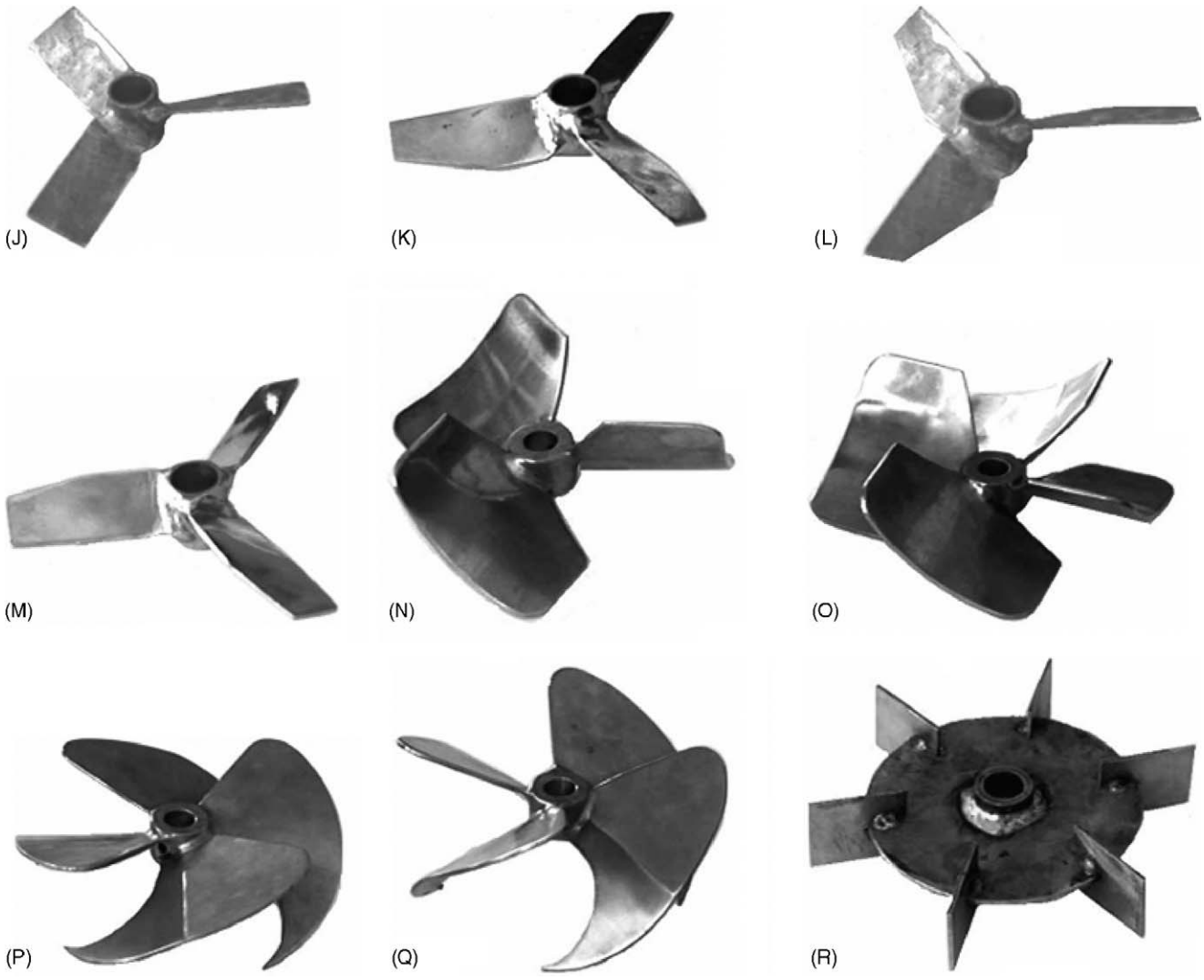

Fig. 1. (*Continued*).

2.3. Flow pattern measurements

The non-invasive velocity measurements were carried out using LDA at four different axial locations (Table 1) following the work of Ranade and Joshi [5]. All the measurements were made at the mid-baffle plane of the vessel. The details of the LDA measurement locations can be seen in Table 1. All the vessel configurations were experimented at an equal power consumption level of 1 kW/m^3. Raw LDA data were preprocessed for the removal of noise following the procedure of Kulkarni et al. [17].

The experimental data of mean axial velocity below the impeller, in the radial direction were used for the calculation of flow numbers. The primary flow number (N_{QP}) and secondary flow number (N_{QS}) were calculated using the following equations:

$$N_{QP} = \frac{\int_0^{R_I} v_z 2\pi r \, dr}{ND^3} \quad (1)$$

$$N_{QS} = \frac{\int_0^{R_R} v_z 2\pi r \, dr}{ND^3} \quad (2)$$

where R_I represents the radius of the impeller and R_R represents the point of reversal of the axial flow.

2.4. CFD simulation

For the prediction of flow pattern, CFD simulation was employed. The turbulence was modeled using a standard k–ε model for which the transport equation for a generalized variable Φ is given by

$$\frac{\partial \Phi}{\partial t} + \frac{1}{r}\frac{\partial}{\partial r}(r v_r \Phi) + \frac{1}{r}\frac{\partial}{\partial \theta}(v_\theta \Phi) + \frac{\partial}{\partial z}(v_z \Phi) = \frac{1}{r}\frac{\partial}{\partial r}\left(r\Gamma\frac{\partial \Phi}{\partial r}\right) + \frac{1}{r}\frac{\partial}{\partial \theta}\left(\frac{\Gamma}{r}\frac{\partial \Phi}{\partial \theta}\right) + \frac{\partial}{\partial z}\left(\Gamma\frac{\partial \Phi}{\partial z}\right) + S_\Phi \quad (3)$$

where Φ stands for v_r, v_z, v_θ, k, ε, etc. The source terms for different flow variables (S_Φ) may be referred from Sahu et al. [18] All the CFD simulations were performed using FLUENT. The total grid size of 443840 ($z \times r \times \theta$: 73 × 32 × 190) was used for the full tank simulation. Impeller region (less than 1.5% of

Table 1
Geometry of impellers investigated, power number, flow number and mixing times

S. no.	Impeller	C/T	D (m)	W/D	D/T	B_{tk} (m)	Axial measurement location (mm)				$N_{P,exp}$	$N_{P,Pred}$	$N_{QP,exp}$	$N_{QS,exp}$	θ_{exp}	θ_{CFD}
							I	II	III	IV						
Pitched blade turbine																
1	PBTD30W5545-3	0.50	0.17	0.32–0.26	0.34	0.003	–	–	–	–	0.63	–	–	–	6.5	–
		0.33	0.17	0.32–0.26	0.34	0.003	25	100	−25	−300	0.66	0.66	0.63	1.58	6.5	6.25
		0.20	0.17	0.32–0.26	0.34	0.003	–	–	–	–	0.75	–	–	–	7.0	–
2	PBTD3020W50-6	0.50	0.17	0.30	0.33	0.003	–	–	–	–	0.62	–	–	–	6.0	–
		0.33	0.17	0.30	0.33	0.003	25	100	−25	−300	0.67	0.69	0.73	1.53	6.5	6.39
		0.20	0.17	0.30	0.33	0.003	–	–	–	–	0.70	–	–	–	7.0	–
3	PBTD30W50-6	0.50	0.17	0.30	0.33	0.002	–	–	–	–	0.63	–	–	–	6.0	–
		0.33	0.17	0.30	0.33	0.002	25	100	−25	−300	0.71	0.70	0.80	1.74	6.0	5.99
		0.20	0.17	0.30	0.33	0.002	–	–	–	–	0.74	–	–	–	7.0	–
4	PBTD60W3085-6	0.50	0.18	0.17–0.48	0.35	0.002	–	–	–	–	3.87	–	–	–	6.0	–
		0.33	0.18	0.17–0.48	0.35	0.002	45	100	−45	−310	3.11	3.08	1.17	2.54	5.5	5.22
		0.20	0.18	0.17–0.48	0.35	0.002	–	–	–	–	3.22	–	–	–	5.5	–
5	PBTD60W50-6	0.50	0.17	0.30	0.33	0.002	–	–	–	–	3.27	–	–	–	5.5	–
		0.33	0.17	0.30	0.33	0.002	30	100	−30	–310	3.30	3.32	1.26	2.43	5.5	5.20
		0.20	0.17	0.30	0.33	0.002	–	–	–	–	3.32	–	–	–	5.5	–
6	PBTD45W50-4	0.50	0.17	0.29	0.35	0.002	–	–	–	–	1.10	–	–	–	6.0	–
		0.33	0.17	0.29	0.35	0.002	30	100	−30	−310	1.30	1.33	0.88	1.85	6.0	5.65
		0.20	0.17	0.29	0.35	0.002	–	–	–	–	1.46	–	–	–	6.5	–
7	PBTD45W30-6	0.50	0.17	0.18	0.34	0.002	–	–	–	–	1.53	–	–	–	7.0	–
		0.33	0.17	0.18	0.34	0.002	30	100	−30	−300	1.44	1.41	1.08	1.90	6.0	5.74
		0.20	0.17	0.18	0.34	0.002	–	–	–	–	1.63	–	–	–	7.0	–
8	PBTD45W50-6	0.50	0.17	0.30	0.33	0.002	–	–	–	–	2.00	–	–	–	5.5	–
		0.33	0.17	0.30	0.33	0.002	+20	+126	−36	−125	2.02	2.00	0.93	2.02	5.50	5.61
		0.20	0.17	0.30	0.33	0.002	–	–	–	–	2.26	–	–	–	6.0	–
9	PBTD45W5030-6	0.50	0.17	0.30–0.18	0.33	0.002	–	–	–	–	2.00	–	–	–	7.0	–
		0.33	0.17	0.30–0.18	0.33	0.002	30	85	−30	−310	1.80	1.76	0.88	1.96	6.0	5.55
		0.20	0.17	0.30–0.18	0.33	0.002	–	–	–	–	2.36	–	–	–	7.0	–
10	PBTD45W3050-6	0.50	0.17	0.18–0.3	0.34	0.003	–	–	–	–	1.74	–	–	–	6.0	–
		0.33	0.17	0.18–0.3	0.34	0.003	30	100	−30	−300	1.69	1.82	1.48	1.95	6.0	5.84
		0.20	0.17	0.18–0.3	0.34	0.003	–	–	–	–	1.82	–	–	–	7.0	–
11	PBTD45W30-6^{S}	0.50	0.10	0.30	0.20	0.002	–	–	–	–	2.00	–	–	–	4.5	–
		0.33	0.10	0.30	0.20	0.002	30	100	−30	−300	2.02	1.9	0.97	1.63	5.0	4.45
		0.20	0.10	0.30	0.20	0.002	–	–	–	–	2.36	–	–	–	6.5	–
12	PBTU45W30-6	0.50	0.10	0.30	0.20	0.002	–	–	–	–	2.21	–	–	–	5.0	–
		0.33	0.10	0.30	0.20	0.002	30	100	−30	−300	2.20	2.20	0.96	2.06	5.5	5.31
		0.20	0.10	0.30	0.20	0.002	–	–	–	–	1.86	–	–	–	6.0	–

Narrow blade hydrofoils																
13	HF30W25-3	0.5	0.167	0.2	0.33	0.003	–	–	–	–	0.25	–	–	–	3.0	–
		0.33	0.167	0.2	0.33	0.003	30	100	30	100	0.27	0.268	0.57	1.01	3.0	2.87
		0.2	0.167	0.2	0.33	0.003	–	–	–	–	0.31	–	–	–	3.5	–
14	HF4500W2517-3	0.5	0.165	0.15–0.1	0.33	0.002	–	–	–	–	0.4	–	–	–	3.0	–
		0.33	0.165	0.15–0.1	0.33	0.002	30	100	30	100	0.38	0.380	0.7	1.03	3.0	2.80
		0.2	0.165	0.15–0.1	0.33	0.002	–	–	–	–	0.42	–	–	–	3.5	–
15	HF45W25-3	0.5	0.14	0.18	0.28	0.002	–	–	–	–	0.34	–	–	–	5.5	–
		0.33	0.14	0.18	0.28	0.002	30	100	30	100	0.33	0.341	0.57	0.79	5.0	5.13
		0.2	0.14	0.18	0.28	0.002	–	–	–	–	0.4	–	–	–	7.5	–
16	HF4530W2517-3	0.5	0.135	0.19–0.13	0.27	0.002	–	–	–	–	0.4	–	–	–	3.0	–
		0.33	0.135	0.19–0.13	0.27	0.002	30	100	30	100	0.41	0.411	0.59	0.96	3.0	3.03
		0.2	0.135	0.19–0.13	0.27	0.002	–	–	–	–	0.46	–	–	–	3.5	–
17	HF6030W2513-3	0.5	0.135	0.19–0.1	0.27	0.002	–	–	–	–	0.32	–	–	–	6.5	–
		0.33	0.135	0.19–0.1	0.27	0.002	30	100	30	100	0.3	0.310	0.58	0.72	6.5	6.38
		0.2	0.135	0.19–0.1	0.27	0.002	–	–	–	–	0.38	–	–	–	8.0	–
18	HF6045W2520-3	0.5	0.134	0.19–0.15	0.27	0.002	–	–	–	–	0.36	–	–	–	3.0	–
		0.33	0.134	0.19–0.15	0.27	0.002	30	100	30	100	0.31	0.300	0.7	1.42	2.5	2.53
		0.2	0.134	0.19–0.15	0.27	0.002	–	–	–	–	0.38	–	–	–	3.0	–
Broad blade hydrofoils																
19	HF2	0.5	0.167	0.5	0.33	0.0025	–	–	–	–	2.12	–	–	–	6.0	–
		0.33	0.167	0.5	0.33	0.0025	45	100	−45	−100	2.32	2.33	1.07	2.01	6.0	5.87
		0.2	0.167	0.5	0.33	0.0025	–	–	–	–	2.41	–	–	–	6.5	–
20	HF3	0.5	0.167	0.5	0.33	0.0025	–	–	–	–	3.26	–	–	–	4.5	–
		0.33	0.167	0.5	0.33	0.0025	45	100	−45	−100	3.34	3.34	1.10	2.24	5.0	4.63
		0.2	0.167	0.5	0.33	0.0025	–	–	–	–	3.52	–	–	–	5.5	–
21	HF3045-4	0.5	0.17	0.8	0.34	0.0025	–	–	–	–	1.75	–	–	–	5.5	–
		0.33	0.17	0.8	0.34	0.0025	50	100	−50	−100	1.78	1.811	0.7	1.27	5.5	5.07
		0.2	0.17	0.8	0.34	0.0025	–	–	–	–	1.8	–	–	–	6.0	–
22	HF4560-4	0.5	0.17	0.8	0.34	0.0025	–	–	–	–	1.48	–	–	–	6.5	–
		0.33	0.17	0.8	0.34	0.0025	50	100	−50	−100	1.53	1.521	0.7	1.01	7.0	6.53
		0.2	0.17	0.8	0.34	0.0025	–	–	–	–	1.62	–	–	–	7.0	–

tank volume) was meshed with 15% of the total grid size used for the full tank in order to resolve the steep gradients in the impeller region. Similarly, near vessel wall and baffle region were meshed with the dense grid. Impeller rotation was modeled using sliding mesh technique except in the simulations for the draft tube configurations. In the sliding mesh simulations, a time step of 0.01 s was employed. The under relaxation parameters used for velocity, pressure, turbulent kinetic energy and energy dissipation were 0.3, 0.6, 0.6 and 0.6, respectively The k–ε model constants C_μ, $C_{\varepsilon 1}$, $C_{\varepsilon 2}$, σ_ε and σ_k were set as 0.09, 1.44, 1.92, 1.3 and 1.0, respectively.

The power consumed by the impeller during stirring should be equal to the power dissipated by the impeller in the liquid. Hence, the impeller power number was calculated from the volume integration of turbulence energy dissipation rate predicated from the CFD model, in the following manner:

$$N_{\mathrm{P,Pred}} = \frac{\int_0^R \int_0^H \int_0^{2\pi} \rho \varepsilon r \, \mathrm{d}r \, \mathrm{d}z \, \mathrm{d}\theta}{\rho N^3 D^5} \tag{4}$$

For the estimation of mixing time, the following transport equation for the concentration c (scalar) was simulated

$$\frac{\partial c}{\partial t} + \frac{1}{r}\frac{\partial}{\partial r}(r v_r c) + \frac{1}{r}\frac{\partial}{\partial \theta}(v_\theta c) + \frac{\partial}{\partial z}(v_z c) = \frac{1}{r}\frac{\partial}{\partial r}\left(r\Gamma\frac{\partial c}{\partial r}\right) + \frac{1}{r}\frac{\partial}{\partial \theta}\left(\frac{\Gamma}{r}\frac{\partial c}{\partial \theta}\right) + \frac{\partial}{\partial z}\left(\Gamma\frac{\partial c}{\partial z}\right) \tag{5}$$

After computation of the velocity and the turbulent kinetic energy profile, the blending process was modeled by solving the conservation equation (5). Here, the dispersive transport of the tracer due to turbulent motion in a stirred vessel is accounted by the turbulent diffusivity, denoted by Γ. The model parameters, grid sizes, and experimental boundary conditions were similar to those used in the prediction of flow pattern. The predicted mixing time using the mixing tine definition based on 98.5% mixing criterion (the time required for $c_{\min}/c_{\max}$ to attain a value of 0.985) was found to be comparable with the mixing time estimated using the conductivity measurement technique for a known impeller. In view of this, the same criterion was employed for the prediction of mixing times for rest of the configurations.

2.5. Estimation of the flow properties

2.5.1. Average shear rate

The shear rate acting on fluid element is given by the deformation tensor. The off diagonal elements of the stress tensor matrix are the shear rates. For cylindrical co-ordinate, these are written in terms of mean velocities as [19]

$$\gamma_{r\theta} = \gamma_{\theta r} = r\frac{\partial}{\partial r}\left(\frac{v_\theta}{r}\right) + \frac{1}{r}\frac{\partial v_r}{\partial \theta} \tag{6}$$

$$\gamma_{\theta z} = \gamma_{z\theta} = \frac{\partial v_\theta}{\partial z} + \frac{1}{r}\frac{\partial v_z}{\partial \theta} \tag{7}$$

$$\gamma_{zr} = \gamma_{rz} = \frac{\partial v_z}{\partial r} + \frac{\partial v_r}{\partial z} \tag{8}$$

The average shear rate (γ_{avg}) in the stirred vessel was calculated by taking summation of the volume average of Eqs. (6)–(8).

2.5.2. Average normal stresses

The turbulent kinetic energy imparted by the impeller in a stirred tank at the desired speed of agitation was calculated by the CFD simulation. The volume averaged turbulent kinetic energy was calculated by the following equations:

$$k_{\mathrm{avg}} = \frac{\int_0^{2\pi} \int_0^H \int_0^R kr \, \mathrm{d}r \, \mathrm{d}z \, \mathrm{d}\theta}{\int_0^{2\pi} \int_0^H \int_0^R r \, \mathrm{d}r \, \mathrm{d}z \, \mathrm{d}\theta} \tag{9}$$

Since $k = (1/2)(v'^2_r + v'^2_\theta + v'^2_z)$ and the individual normal stresses are v'^2_r, v'^2_θ, v'^2_z, respectively. The average normal stress is given by the following equation:

$$\bar{\tau}_{\mathrm{N}} = \tfrac{2}{3}\rho k_{\mathrm{avg}} \tag{10}$$

3. Results and discussion

3.1. Pitched blade turbines

The effect of impeller diameter ($D/T = 0.2$, 0.33, 0.34 and 0.35), blade angle (30°, 45°, and 60°), number of blades (3, 4 and 6), blade width (W/D from 0.18 to 0.3), blade twist (10°) and principal flow direction (downflow/upflow) are studied on the flow pattern prevailing in the stirred tank.

3.1.1. 30° pitched blade turbine

Experiments have been performed on three different types of 30° pitched blade downflow turbines at constant power consumption level of 1 kW/m^3, which are modified in their blade designs. One of the impellers is three-bladed with progressive reduction in blade width (PBTD30W5545-3) from the impeller hub (55 mm) to blade tip (45 mm) whereas other two impellers are six-bladed in which one of them had 10° blade twist (PBTD3020W50-6) near the blade tip and other one is with constant blade width (PBTD30W50-6) of 50 mm. The comparisons of mean radial velocity profiles near the vessel base ($z/R = 0.4$) and below the impeller ($z/R = 0.1$) are shown in Fig. 2A and B, respectively. The radial velocity for the pitched blade turbine with three blades (PBTD30W5545-3) was found lesser ($0.25 \geq r/R \geq 0.8$) than the six straight bladed impeller (Fig. 2A). However, the difference in the magnitude of radial velocity was clearly observed in the impeller vicinity, immediately below the impeller (Fig. 2B). The radial velocity for the six straight bladed impeller was found to be maximum ($0.05U_{\mathrm{tip}}$) at $r/R = 0.22$ whereas the magnitude reduced to $0.038U_{\mathrm{tip}}$ and $0.02U_{\mathrm{tip}}$ for the six-bladed impeller with 10° blade twist and three-bladed impeller, respectively. However, near the vessel periphery, the strength of inward radial flow was found to be higher ($0.01U_{\mathrm{tip}}$) at $0.4 \geq r/R \geq 0.9$ ($z/R = 0.1$) for the impeller with 10° blade twist (Fig. 2B).

Fig. 2C and D shows the comparisons of the mean axial velocity for 30° pitched blade turbine at two axial locations, which show a negligible difference in the axial velocity trends. Near the vessel base ($z/R = 0.4$), the axial velocity of the three-

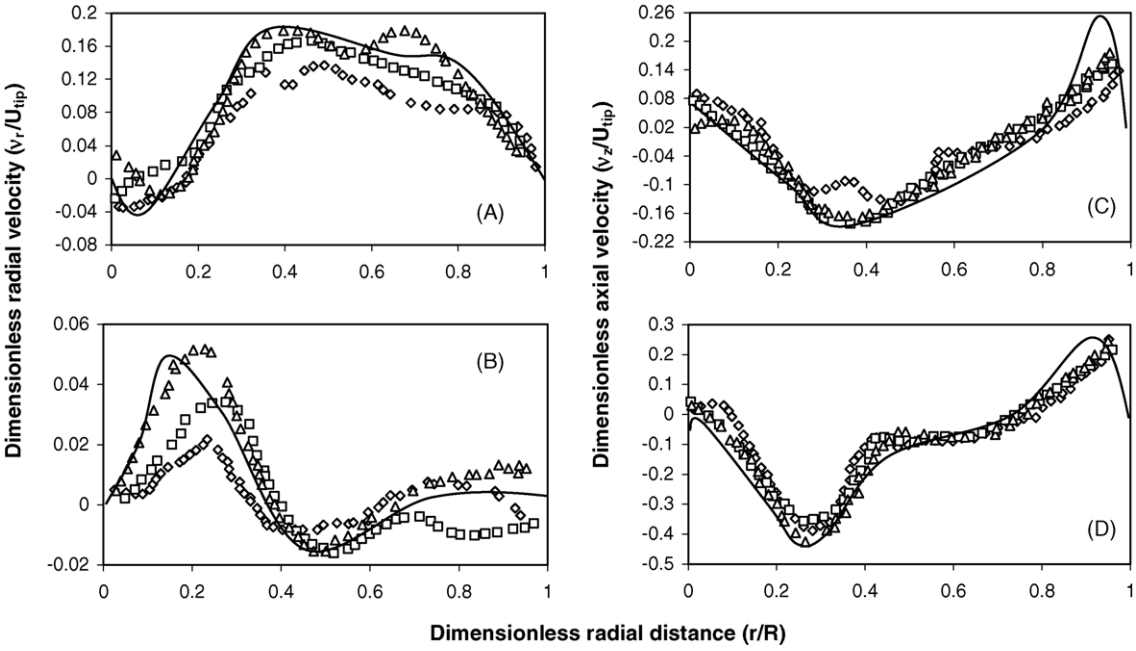

Fig. 2. Mean radial and axial velocities generated by 30° pitched blade turbine. (A and C) Near the vessel base; (B and D) below impeller; (◊) PBTD30W5545-3; (□) PBTD3020W50-6; (△) PBTD30W50-6; (—) CFD-PBTD30W50-6.

bladed impeller was found to be slightly lesser than that of the six-bladed impellers (Fig. 2C). Below the impeller ($z/R = 0.1$), the six-bladed impeller with constant blade width gave a maximum axial flow (Fig. 2D) of $0.42U_{tip}$ at $r/R = 0.25$. Ranade et al. [20] observed that the maximum axial velocity of $0.38U_{tip}$ at $r/R = 0.28$ and $z/R = 0.12$. The quantitative difference in axial velocity beyond $r/R \geq 0.3$ was negligible. However, the 30° impeller's flow efficiencies can be seen from Table 1. The N_{QP} is minimum (0.63) for three-bladed impeller and maximum (0.8) for impeller with constant blade width. The secondary flow number for the impeller with 10° blade twist is lesser than the impeller with straight blades, which implies that the presence of blade twist in the six-bladed 30° pitched blade impeller, has poor entrainment of liquid towards the vessel core ($N_{QS} = 1.53$). The CFD predictions below the impeller ($z/R = 0.1$) show an excellent comparison with the LDA measurements. Similarly, the mixing time was found to be minimum ($\theta_{CFD} = 5.99$ s) for PBTD30W50-6 with good entrainment ($N_{QS} = 1.74$). Patwardhan and Joshi [1] have observed that the mixing time could be well correlated with the help of secondary flow number rather than the primary pumping capacity. This implies that the total flow (N_{QS}) must be taken into consideration.

Fig. 3A and B shows the comparisons of the mean tangential velocity near the vessel base ($z/R = 0.4$) and below the impeller ($z/R = 0.1$). Near the vessel base (Fig. 3A), the tangential velocity profiles are not consistent with the change in the impeller blade design. The CFD prediction for PBTD30W50-6 is over predicted at $r/R \leq 0.6$ and under predicted at $r/R \geq 0.6$. At $0.2 \geq r/R \leq 0.4$, in the direction of the impeller motion, the swirling velocity was found to be maximum ($0.08U_{tip}$ at $z/R = 0.4$) for the three-bladed impeller. However, the tangential velocities are dominant and found to be stronger below the impeller (Fig. 3B), which shows the presence of strong vortex below the 30° pitched blade turbines ($r/R \leq 0.2$). The observed magnitude below ($z/R = 0.1$, $r/R = 0.2$) the constant blade width impeller (PBTD30W50-6) is $0.16U_{tip}$. However, below the impeller, the difference in the tangential velocity was found to be significant in the vessel core region ($r/R \leq 0.2$).

Fig. 3C and D shows the comparisons of the turbulent kinetic energy near the vessel base ($z/R = 0.4$) and below the impeller ($z/R = 0.1$) for the 30° pitched blade turbine, respectively. The differences in kinetic energy profiles are distinct at $r/R \leq 0.4$. The maximum value of turbulent kinetic energy was for the impeller with constant blade width near the vessel base ($0.043U_{tip}^2$) and below the impeller ($0.1U_{tip}^2$) at $r/R = 0.2$. However, near the vessel base ($z/R = 0.4$), the CFD prediction for the straight blade impeller (PBTD30W50-6) under predicted the turbulent kinetic energy level to about 50% at $r/R \geq 0.4$. The power measurements reveal that the power number for the impeller with constant blade (PBTD30W50-6) width was higher ($N_{P,exp} = 0.71$) than other two 30° impellers considered in this study. The N_P values are found to be minimum for three-bladed PBTD (0.66) and six-bladed impeller with blade twist (0.67). Table 2 shows the effect of impeller design on the turbulence properties. The location and the value of ε_{max} depend upon the impeller design and the other geometrical parameters. At 1 W/kg of P/V, different impellers produce different levels of ε_{max} (Table 2). The estimated values of dimensionless ε_{max}/N^3D^2 for PBTD30W5545-3, PBTD3020W50-6 and PBTD30W50-6 were 2.104, 2.128 and 2.145, respectively. Of the total fluctuations, the participation of axial fluctuating velocity (u_z') is almost 90–92% near the impeller zone. The axial–radial shear stress was found to be higher in the case of axial flow impellers, where γ_{avg} increases with the increase in both the gradients of mean axial and radial velocities ($\partial vz/\partial z$) and ($\partial vr/\partial z$). However, γ_{avg} was found to be higher ($1.757\ s^{-1}$) for PBTD30W50-6.

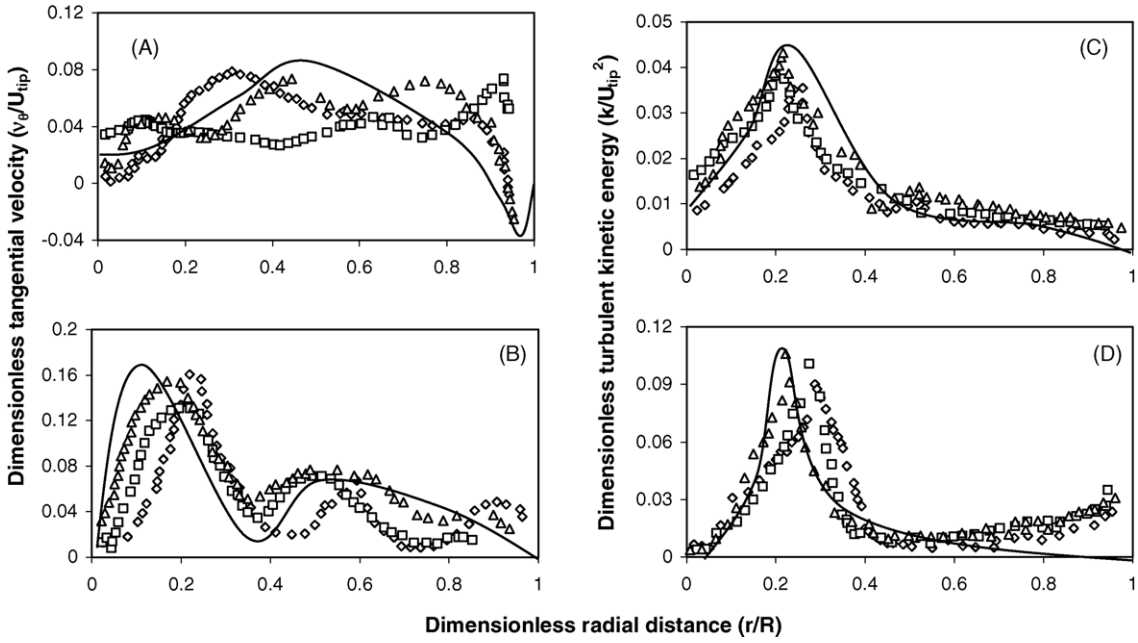

Fig. 3. Mean tangential velocity and turbulent kinetic energy pattern by 30° pitched blade turbine. (A and C) Near the vessel base; (B and D) below impeller; (◊) PBTD30W5545-3; (□) PBTD3020W50-6; (△) PBTD30W50-6; (—) CFD-PBTD30W50-6.

3.1.2. 60° pitched blade turbine

Two types of 60° pitched blade impellers were taken for the measurements; one impeller was with increasing blade width (PBTD60W3085-6) from impeller hub ($W = 30$ mm) to blade tip ($W = 85$ mm) and other one with constant blade width (PBTD60W50-6). Fig. 4A and B shows the effect of blade width on the mean radial velocity. Near the vessel base ($z/R = 0.14$), the impeller with constant blade width was found to provide more strength ($0.26U_{tip}$) in pumping the fluid radially at $r/R = 0.5$ (Fig. 4A) whereas the impeller with increasing blade width (PBTD60W3085-6) at the same radial location gave $0.17U_{tip}$ that is 35% lesser in magnitude. This was in good agreement with the work of Ranade and Joshi [5] where the maximum mean radial velocity for the constant blade width ($W/D = 0.33$) impeller was $0.25U_{tip}$. Below the impeller, both PBTD60W3085-6 ($z/R = 0.18$) and PBTD60W50-6 ($z/R = 0.12$) experienced a similar trend in the mean radial profile as shown in Fig. 4B. The impeller with increasing blade width occupies more impeller volume, hence, axial location of measurement was at $z/R = 0.18$. The mean radial velocity reaches a

Table 2
Effect of impeller design on primary and secondary flow numbers, maximum energy dissipation rate, average turbulent normal stress and average shear rates

Impeller	D (m)	W/D	D/T	B_{tk} (m)	$N_{P,Pred}$	$N_{QP,CFD}$	$N_{QS,CFD}$	N (rps)	ε_{max} (kW/m^3)	ε_{max}/N^3D^2	$\overline{\tau}_N$ (N/m^2)	γ_{avg} (1/s)	k_{avg} (m^2/s^2)
PBTD30W5545-3	0.168	0.32–0.26	0.34	0.003	0.66	0.64	1.52	10.37	66.279	2.104	56.29	1.647	0.084
PBTD3020W50-6	0.165	0.3	0.33	0.003	0.69	0.72	1.50	10.50	67.094	2.128	59.38	1.737	0.089
PBTD30W50-6	0.165	0.3	0.33	0.002	0.70	0.78	1.68	10.46	66.838	2.145	60.07	1.757	0.090
PBTD60W3085-6	0.175	0.17–0.48	0.35	0.002	3.08	1.16	2.52	5.79	30.980	5.218	75.51	7.731	0.113
PBTD60W50-6	0.165	0.3	0.33	0.002	3.32	1.22	2.41	6.23	33.328	5.072	81.40	8.333	0.122
PBTD45W50-4	0.173	0.29	0.35	0.002	1.33	0.86	1.83	7.81	49.869	3.504	32.61	3.338	0.049
PBTD45W30-6	0.168	0.18	0.34	0.002	1.41	1.03	1.85	8.04	51.358	3.504	34.57	3.539	0.052
PBTD45W50-6	0.17	0.3	0.33	0.002	1.8	0.93	2.02	10.26	48.19	1.544	90.67	2.82	0.136
PBTD45W5030-6	0.165	0.3	0.33	0.002	1.76	0.85	1.93	7.55	48.239	4.117	45.65	4.674	0.068
PBTD45W3050-6	0.168	0.18–0.3	0.34	0.0025	1.82	1.46	1.97	7.52	48.066	4.000	42.17	4.317	0.063
PBTD45W30-6	0.1	0.3	0.2	0.002	1.86	0.99	1.67	15.96	102.922	2.531	29.54	3.025	0.044
PBTU45W30-6	0.1	0.3	0.2	0.002	2.20	0.96	2.03	16.45	99.980	2.244	26.97	2.761	0.040
HF30W25-3	0.167	0.2	0.33	0.003	0.27	0.55	1.00	14.12	84.902	1.081	6.57	0.673	0.010
HF4500W2517-3	0.165	0.15–0.1	0.33	0.002	0.38	0.71	1.02	12.82	77.106	1.343	9.32	0.954	0.014
HF45W25-3	0.14	0.18	0.28	0.002	0.34	0.55	0.79	17.48	105.122	1.004	8.36	0.856	0.013
HF4530W2517-3	0.135	0.19–0.13	0.27	0.002	0.41	0.61	0.94	17.45	104.951	1.083	10.08	1.032	0.015
HF6030W2513-3	0.135	0.19–0.1	0.27	0.002	0.31	0.59	0.72	19.17	115.296	0.897	7.60	0.778	0.011
HF6045W2520-3	0.134	0.19–0.15	0.27	0.002	0.30	0.71	1.36	19.63	118.017	0.869	7.36	0.753	0.011
HF2	0.167	0.5	0.33	0.0025	2.33	1.05	2.00	6.87	11.541	1.278	19.99	5.848	0.030
HF3	0.167	0.5	0.33	0.0025	3.34	1.12	2.26	6.09	10.236	1.625	28.66	8.383	0.043
HF3045-4	0.17	0.8	0.34	0.0025	1.81	0.70	1.31	7.25	12.185	1.106	15.54	4.546	0.023
HF4560-4	0.17	0.8	0.34	0.0025	1.52	0.71	1.04	7.68	12.915	0.985	13.05	3.818	0.020

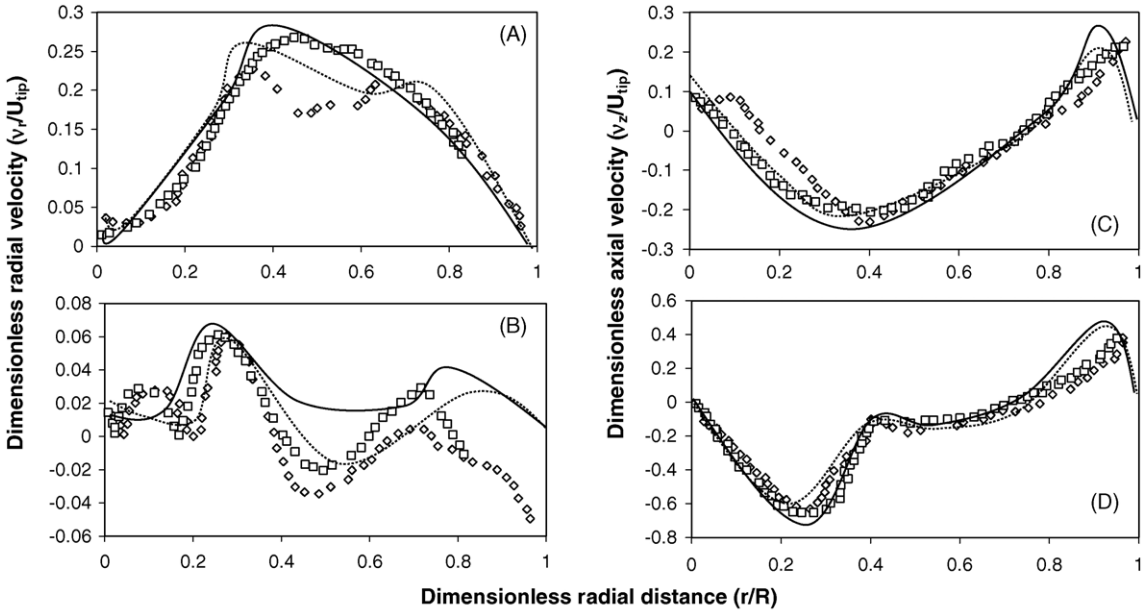

Fig. 4. Mean radial and axial velocities generated by 60° pitched blade turbine. (A and C) Near the vessel base; (B and D) below impeller; (◊) PBTD60W3085-6; (□) PBTD60W50-6; (···) CFD-PBTD60W3085-6; (—) CFD-PBTD60W50-6.

maximum of $0.06U_{tip}$ for PBTD60W3085-6 at $z/R = 0.1$ and $r/R = 0.27$. The CFD results over predicted in the vessel core region ($0.3 \geq r/R \geq 0.75$).

Fig. 4C and D shows the effect of blade width on the mean axial velocity at two axial locations. Major difference in magnitude was not seen in mean axial velocity near the vessel base and below the impeller. Below the impeller ($z/R = 0.12$; Fig. 4D), the axial velocity of PBTD60W50-6 was found higher ($0.65U_{tip}$) than the impeller with increasing blade (PBTD60W3085-6) width at the vessel core region ($r/R < 0.3$). Ranade and Joshi [5] observed the maximum axial velocity for the impeller with constant blade width ($W/D = 0.3$), near the vessel base as $0.38U_{tip}$ (at $z/R = 0.366$ and $r/R = 0.3$). Similarly, Hockey and Nouri [21] observed the maximum magnitude to be $0.55U_{tip}$ below the impeller ($z/R = 0.14$ for $W/D = 0.18$). The axial flow jet from the impeller base is higher for the 60° blade pitch with constant blade width. The N_{QP} and N_{QS} for the constant blade width impeller were found to be 1.26 and 2.43, respectively (Table 1). However, the primary flow number for PBTD60W50-6 increased to about 7% than impeller with increasing blade width (PBTD60W3085-6). Similarly, CFD predictions show increased level of mean axial flow for PBTD60W50-6 especially near the impeller zone. Since there is no marginal difference in the axial flow, the predicted mixing time was found to be almost the same ≈5.2 s (Table 1).

Fig. 5A and B shows the mean tangential velocity near the vessel base ($z/R = 0.4$) and below the impeller ($z/R = 0.12$), respectively. Below the impeller and near to the vessel base, the trend for the mean tangential velocity is almost same at $r/R \leq 0.3$. However, there is a slight difference away from the vessel core region ($r/R \geq 0.3$) where the tangential velocity profile was slightly higher for constant blade width impeller (PBTD60W50-6) at $0.3 \geq r/R \leq 0.6$ (Fig. 5B). The PBTD60W50-6 experiences a reversible tangential flow (≈$0.15U_{tip}$ at $r/R \geq 0.8$) near the vessel edge in the impeller mid-plane region (Fig. 5A). The CFD predictions however, reveal such reversible swirls in both the 60° pitched blade impellers. Below the constant blade width impeller (Fig. 5B), the maximum value of the swirling component was found to be $0.43U_{tip}$ at $r/R = 0.22$ and $z/R = 0.12$, whereas Hockey and Nouri [21] observed a peak value of $0.5U_{tip}$ at $r/R = 0.3$ and $z/R = 0.14$.

Fig. 5C and D shows the turbulent kinetic energy profiles at $z/R = 0.4$ and 0.12, respectively. At all the four axial locations ($z/R = 0.12$, 0.4, −0.12 and −1.24), the turbulent kinetic energy profile for the PBTD60W50-6 was always greater than the impeller with increasing blade width (PBTD60W3085-6). The predicted turbulent kinetic energy at $r/R = 0.3$ was 16% higher in magnitude for the constant blade width impeller (PBTD60W50-6). Below the impeller (Fig. 5D), the maximum value of turbulent kinetic energy ($0.12U_{tip}^2$) at $r/R = 0.3$ is in good agreement with Ranade et al. [20] This is well reflected in the power number measurement using load cell setup. The N_P for PBTD60W50-6 is 3.30, which is 5.7% higher than the impeller with varying blade width. The predicted overall turbulent kinetic energy ($0.122\ m^2/s^2$) for PBTD60W50-6 was higher than the impeller with varying blade width. The overall kinetic energy dissipation rate for PBTD60W50-6 was found to be $33.33\ m^2/s^3$. Even though, there was only slight difference in the mean axial velocity, it reflected in the overall normal stress ($81.4\ N/m^2$) that is 7% higher for PBTD60W50-6.

3.1.3. 45° pitched blade turbine

Seven types of 45° pitched blade turbines with modified blade designs were taken for the experimentation. The effect of impeller diameter, pumping direction, blade width and number of blades on the flow pattern is studied. Fig. 6A and B shows the

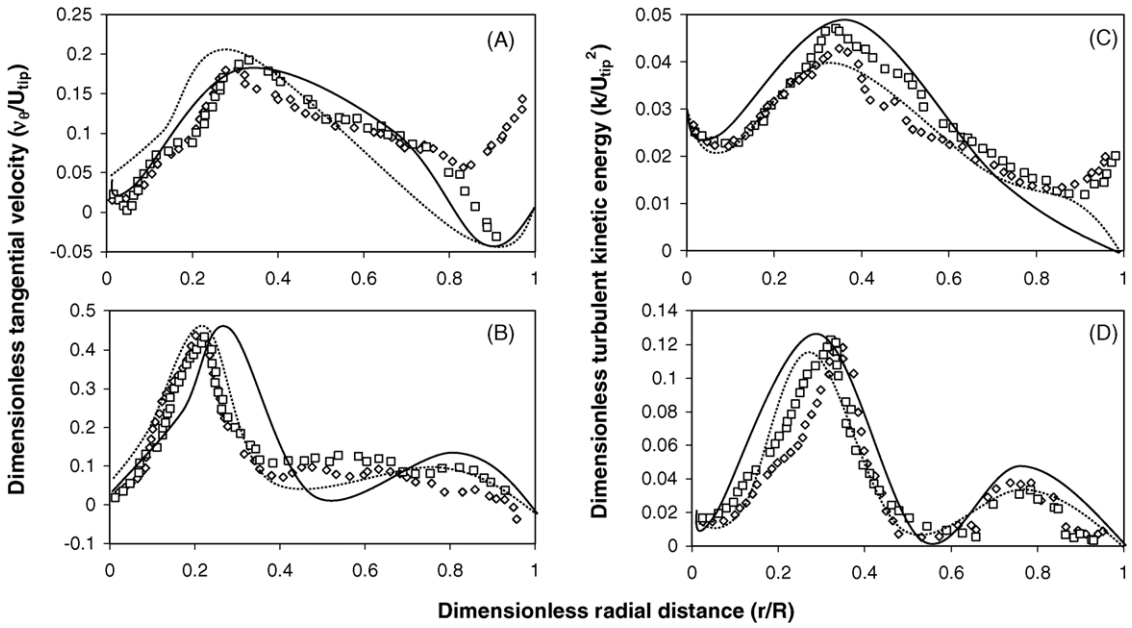

Fig. 5. Mean tangential velocity and turbulent kinetic energy pattern by 30° pitched blade turbine. (A and C) Near the vessel base; (B and D) below impeller; (◊) PBTD60W3085-6; (□) PBTD60W50-6; (···) CFD-PBTD60W3085-6; (—) CFD-PBTD60W50-6.

comparisons of the mean radial velocity for 45° pitched blade turbine at two axial locations. Near the vessel base ($r/R = 0.4$ and $z/R = 0.4$), the mean radial velocity for the four blade pitched blade turbine (PBTD45W50-4) is the highest ($0.27U_{tip}$) of all 45° pitched blade turbines used in this study. The six straight blade pitched blade turbine ($D/T \approx 0.3$), PBTD45W30-6, PBTD45W50-6 and PBTD45W5030-6 reached to $0.2U_{tip}$, $0.12U_{tip}$ and $0.16U_{tip}$ (Fig. 6A) at $r/R = 0.4$ and $z/R = 0.4$, respectively, whereas the impeller with increasing blade width (PBTD45W3050-6) shows less than $0.1U_{tip}$. It is also interesting to note that downflow impeller with D/T ratio of 0.2 (PBTD45W30-6^S) experiences a reversible radial flow near the corner ($r/R \geq 0.75$) of the vessel base whereas the upflow impeller with D/T ratio of 0.2 show a bulk movement of inward radial flow, which is stronger ($0.14U_{tip}$ at $r/R = 0.12$) in the vessel core region. The CFD prediction for the impeller with decreasing blade width (PBTD45W5030-6) matches well with the LDA measurements. The presence of such reversible radial flow near

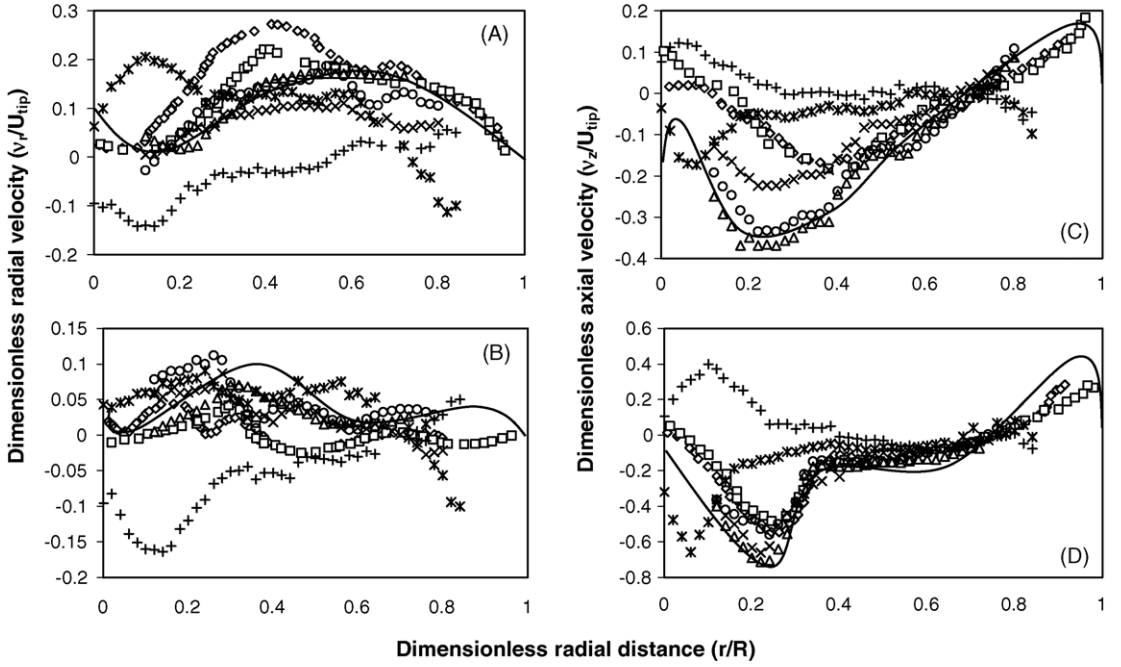

Fig. 6. Mean radial and axial velocities generated by 45° pitched blade turbine. (A and C) Near the vessel base; (B and D) below impeller; (◊) PBTD45W50-4; (□) PBTD45W30-6; (△) PBTD45W5030-6; (×) PBTD45W3050-6; (✱) PBTD45W30-6^S; (+) PBTU45W30-6; (◯) PBTD45W50-6; (—) CFD-PBTD45W50-6.

the vessel corners may be disadvantage for solid suspension operation and slurry reactors due to the formation of stagnant zones in the reactor. Below the impeller (Fig. 6B), at $z/R = 0.12$, the range of radial velocities are lesser than $0.1U_{tip}$. Kresta and Wood [22] observed a maxima ($0.15U_{tip}$) for the four bladed 45° pitched blade downflow impeller ($W/D = 0.18$) at $r/R = 0.3$ and $z/R = 0.08$ which is in good agreement with the present work. However, the mean radial velocity for the upflow impeller (PBTU45W30-6) reached $0.16U_{tip}$ at $r/R = 0.12$. This is because of the lesser energy dissipation below the impeller and due to the bulk movement of the inward radial flow towards the impeller core. A very similar behavior was observed above the impeller for PBTU45W30-6 that the energy dissipation rate is very less due to the free flow of the axial jet above the impeller. The radial velocity profile above the impeller and near to the liquid surface is not shown for brevity. The radial velocity magnitudes for other 45° pitched blade impellers are less than $0.1U_{tip}$.

Fig. 6C and D shows the comparisons of the mean axial velocity for 45° pitched blade turbine at two axial locations. Near the vessel base (Fig. 6C), at $z/R = 0.4$, the magnitude of the axial velocity is about $0.361U_{tip}$ (at $r/R = 0.24$) for the impeller with decreasing blade width from impeller hub to blade tip (PBTD45W5030-6). Similar trend ($0.7U_{tip}$ at $r/R = 0.24$) was observed for the axial velocity below PBTD45W5030-6 (Fig. 6D). Apart from all the 45° pitched blade impellers experimented, the impeller with decreasing blade width from impeller hub to blade tip (PBTD45W5030-6) gave maximum axial flow of $0.7U_{tip}$ at $r/R = 0.24$ and $z/R = 0.12$ (Fig. 6D). However, the impeller with increasing blade width also attains a magnitude of $0.66U_{tip}$ at the same radial and axial location, which is 6% lesser than that of PBTD45W5030-6 whereas PBTD45W50-6 was with $0.5U_{tip}$ at $r/R = 0.24$ and $z/R = 0.12$, which is lesser than the impeller with changing blade width (PBTD45W5030-6 and PBTD45W3050-6). The $N_{QP,exp}$ value for PBTD45W5030-6 and PBTD45W3050-6 was found to be 0.88 and 1.48, respectively. However, the four-bladed pitched blade turbine (PBTD45W50-4) and six-bladed pitched blade turbine with smaller blade width (PBTD45W30-6) attained a maximum axial velocity of $0.5U_{tip}$ at $z/R = 0.12$ and $r/R = 0.25$. Zhou and Kresta [15] observed a maxima ($0.358U_{tip}$) for the four-bladed 45° pitched blade downflow impeller ($W/D = 0.18$) at $r/R = 0.3$ and $z/R = 0.04$. The increase of axial velocity in the four-bladed impeller (PBTD45W50-4) is due to the 40% increase in blade width. Apart from all the impellers with 45° blade pitch, the downflow impeller with smaller D/T ratio (PBTD45W30-6) gives the minimum secondary flow number (1.63) indicating the poor entrainment of liquid. The magnitude of the axial velocity for PBTD45W30-6^S at $z/R = 0.12$ is about $0.66U_{tip}$ at $r/R = 0.06$ (Fig. 6D). The maximum value shifted towards the impeller core region for PBTD45W30-6^S is due to the smaller D/T ratio ($D/T = 0.2$). The flow numbers for the upflow impeller (PBTU45W30-6) is calculated from the axial velocity profile above the impeller ($z/R = -1.2$) where N_{QP} (0.96), which is almost 53% lesser than the N_{QS} (2.06). The predicted mixing time for PBTD45W30-6^S was found to be 4.45 s that is minimum than all other 45° blade pitched impellers performed.

Fig. 7A and B shows the comparisons of the mean tangential velocity for 45° pitched blade turbine at two axial locations ($z/R = 0.12$ and 0.4). Near the vessel base (Fig. 7A), the magnitude of tangential velocity for PBTD45W30-6^S was found to be $0.14U_{tip}$ at $z/R = 0.4$ and $r/R = 0.4$. At the same radial and axial location, the upflow impeller (PBTU45W30-6) attained a minimum tangential velocity of $0.08U_{tip}$. However, the standard 45° impeller (PBTD45W50-6) attains a maximum tangential velocity of $0.16U_{tip}$ at $z/R = 0.4$ and $r/R = 0.3$. A similar trend was observed for mean tangential velocity below the impeller ($z/R = 0.12$). Below the impeller (Fig. 7B), the tangential component is higher for the four-bladed impeller ($0.28U_{tip}$) at $z/R = 0.12$ and $r/R = 0.2$ whereas the impeller with changing blade width (PBTD45W5030-6 and PBTD45W3050-6) shifted its maximum tangential velocity ($0.24U_{tip}$) to $r/R = 0.3$ at $z/R = 0.12$. The maximum tangential velocity in the case of four-bladed impeller ($W/D = 0.14$) was found to be $0.2U_{tip}$ in the work of Kresta and Wood [22] at $z/R = 0.08$ and $r/R = 0.33$. Rather than six-blade pitched blade turbine (PBTD45W50-6), the macroinstability frequency was dominated by the four-blade pitched blade turbine (PBTD45W50-4) [23]. The downflow impeller with smaller D/T ratio (PBTD45W30-6^S) attained a maximum tangential velocity of $0.28U_{tip}$ at $z/R = 0.12$ and $r/R = 0.2$. This indicates that the 45° pitched blade downflow turbine with straight blades (no change in blade width) attains a maximum swirling flow below the impeller.

Fig. 7C and D shows the comparisons of the turbulent kinetic energy for all the 45° pitched blade turbines at two axial locations. Near the vessel base ($z/R = 0.4$), the magnitude of the four-bladed turbine (PBTD45W50-4) attained $0.028U_{tip}^2$ at $r/R = 0.35$, which is maximum for all 45° pitched blade turbines (Fig. 7C). Similarly the maximum value for six-bladed turbine (PBTD45W30-6) with smaller blade width ($W/D = 0.18$ and $D/T = 0.34$) is seen to be at $z/R = 0.4$ and $r/R = 0.28$. However, the impeller with change in blade width (PBTD45W5030-6 and PBTD45W3050-6) and the downflow impeller with smaller D/T ratio (PBTD45W30-6^S) attains the maximum value ($0.032U_{tip}^2$) at $z/R = 0.4$ and $r/R = 0.14$. Below the impeller (Fig. 7D), at $z/R = 0.12$, all 45° pitched blade turbines, which has higher D/T ratios (0.33, 0.34 and 0.35) attains a maximum turbulent kinetic energy at $r/R = 0.3$. However, impeller with the changing blade width attains a maximum value of $0.09U_{tip}^2$ at $z/R = 0.12$ and $r/R = 0.3$. The impeller with smaller D/T ratio (PBTD45W30-6 and PBTU45W30-6) reaches maximum ($0.092U_{tip}^2$) at $z/R = 0.12$ and $r/R = 0.18$. This is due to effect of smaller impeller diameter that has narrow jet emerging from the impeller. However the maximum level of turbulent kinetic energy reached by the upflow impeller (PBTD45W30-6) is 22% lesser than the downflow impeller (PBTU45W30-6) at $z/R = 0.12$ and $r/R = 0.18$. Since the impeller frequency was higher for smaller D/T ratio, the predicted maximum energy dissipation rate near the impeller was found to be higher for PBTD45W30-6 (102.92 m^2/s^3) and PBTU45W30-6 (99.98 m^2/s^3). The overall normal stress was found maximum (90.67 N/m^2) for the standard 45° impeller (PBTD45W50-6). The average shear rate was higher (≈4.5) for the impeller with changing blade width (PBTD45W5030-6 and PBTD45W3050-6).

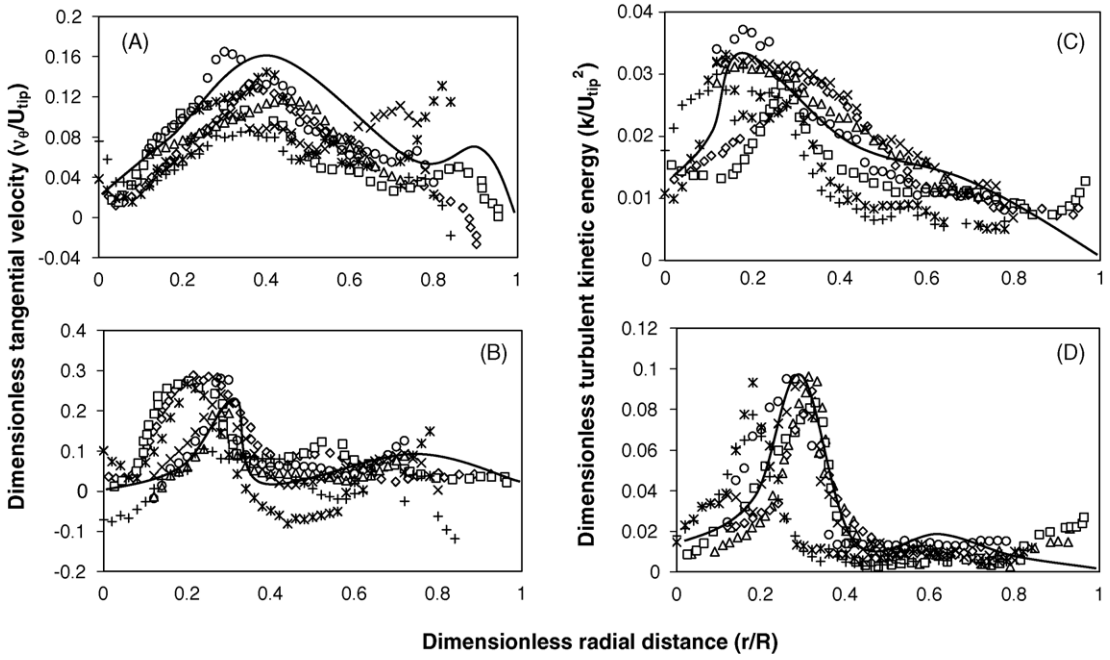

Fig. 7. Mean tangential velocity and turbulent kinetic energy pattern by 45° pitched blade turbine. (A and C) Near the vessel base; (B and D) below impeller; (◊) PBTD45W50-4; (□) PBTD45W30-6; (△) PBTD45W5030-6; (×) PBTD45W3050-6; (✱) PBTD45W30-6^S; (+) PBTU45W30-6; (◯) PBTD45W50-6; (—) CFD-PBTD45W50-6.

The effect of blade angle, blade twist, impeller diameter, blade width and number of blades on the pitched blade turbine was investigated. Conclusively, it can be outlined as follows.

3.1.3.1. Effect of blade angle. From Table 1, it can be concluded that the power number (N_P) is higher for the impeller with maximum pitch (60°) that reaches a maximum turbulent kinetic energy level of $0.12U_{tip}^2$ at $z/R = 0.12$ and $r/R = 0.3$. From Table 2, it can be seen that as the blade angle increases, the primary flow number (N_{QP}), secondary flow number (N_{QS}), and the power number (N_P) increase for the standard impeller design. The N_{QS}/N_{QP} ratio was found to be 2.15 and 2.17 for 30° and 45° pitch, respectively, whereas it reduced to 1.73 for 60° pitched blade impeller. However, the N_{QS}/N_P ratio gradually decreases with increasing pitch from 30° (2.4) to 60° (0.72). The average shear rate for 60° pitched impeller is almost 4.5 times the shear level of 30° pitched blade impellers (Table 2). When compared on the basis of equal power consumption level of 1 kW/m^3, the mixing time reduces with the increase in blade pitch.

3.1.3.2. Effect of blade width. The effect of blade width was investigated in two ways. In the first case, the blade width was progressively decreased from $W/D = 0.32$ at the hub to $W/D = 0.26$ at the impeller tip (PBTD30W5545-3 and PBTD45W5030-6) or progressively increased $W/D = 0.16$ at the hub to $W/D = 0.47$ at the impeller tip (PBTD60W3085-6 and PBTD45W3050-6). Irrespective of the impeller blade pitch, the change in blade width reduces the power number. However, the flow numbers are not consistent with the change in the impeller blade width and the effect of mixing time is not straightforward. For the 45° impeller, the mixing time is almost same that is only 1% decrease in mixing time is observed with the progressive decrease in blade width whereas in the case of 30° impeller, the value of mixing time increased by 4%. At the same time, irrespective of the impeller blade pitch, the progressive increase in blade width increase the mixing time by 4%.

In the second case, there is no progressive variation in the blade width from hub to impeller tip. Instead, two more W/D ratios (0.18 and 0.3) were investigated on 45° pitched blade (PBTD45W30-6, PBTD45W50-6). It was observed that power number decrease with the decrease in W/D ratio. The N_{QP} increase (14%) with the decrease in blade width from 0.3 to 0.18 whereas there is only slight decrease (6%) in N_{QS}.

3.1.3.3. Effect of blade twist. The effect of blade twist was performed with the 30° blade pitch (PBTD3020W50-6 and PBTD30W50-6). It was observed that the presence of blade twist (PBTD3020W50-6) decreases the power number and flow numbers. It can be observed that there is 3% reduction in secondary flow number in the presence of 10° blade twist. The averaged shear rate decrease slightly (1%) in the presence of 10° blade twist.

3.1.3.4. Effect of impeller diameter. The effect of impeller diameter was investigated on the 45° impeller (PBTD45W50-6 ($D/T = 0.34$, $W/D = 0.3$) and PBTD45W30-6 ($D/T = 0.2$, $W/D = 0.3$)) with constant W/D ratio. It was found that both power number and flow number increase with the decrease in impeller diameter. As the impeller diameter increases from $D/T = 0.2$ to 0.3, the mixing time increases by 20%. On the other hand, the effect of impeller diameter was investigated on the 45° impeller (PBTD45W30-6 ($D/T = 0.34$, $W/D = 0.18$) and PBTD45W30-6 ($D/T = 0.2$, $W/D = 0.3$)) with varying blade width. The mixing time increase (22%) with the increase in

impeller diameter along with increase (50%) in W/D ratio. The N_P, N_{QP} and N_{QS} increase with the increase in impeller diameter to about 25%, 10% and 14%, respectively.

3.1.3.5. Effect of pumping direction. The effect of changing the pumping direction was studied for the 45° pitched blade of D/T ratio of 0.2 (PBTD45W30-6^S and PBTU45W30-6). For a downflow impeller, the jet leaving the impeller interacts with the vessel base, producing more energy dissipation in the region below the impeller. For an upflow impeller, the jet leaving the impeller interacts with the top liquid surface, where the energy dissipation will be comparatively smaller. This is in good agreement with the CFD predictions of Patwardhan and Joshi [1]. The average shear rate was also 8% higher for the downflow impeller.

3.1.3.6. Effect of number of blades. The effect of number of blades was investigated on the 45° impeller (PBTD45W50-4 and PBTD45W50-6). With the increase in number of blades from four to six, both power number and flow number increased. The N_P, N_{QP} and N_{QS} increase to about 26%, 8% and 10%, respectively. The average normal stress increase to about 64% with the increase in number of blades from four to six.

3.2. Narrow bladed hydrofoils

The axial flow impellers especially the narrow bladed hydrofoils are very much sensitive to the blade twist and blade width. Generally, the part of input power that is not used in generating head or flow is dissipated through shear or turbulent eddies. However, this dissipation of turbulent kinetic energy is not necessarily harmful because there are some applications like mixing of immiscible fluids, suspension of solids, gas dispersion etc. need such turbulent eddies or vortices to attain desired end product. The hydrofoils are mean to be high efficient blades that accounts for lesser energy dissipation and greater production of flow or head. The D/T ratio of narrow bladed hydrofoils ranged from 0.27 to 0.33 in the present study. In the present study, the effect of impeller diameter, blade width, blade twist and blade pitch on the flow pattern were investigated. However, the number of blades was maintained constant (three blades) for all the narrow bladed hydrofoils.

Fig. 8A and B shows the comparisons of the mean radial velocity for the narrow bladed hydrofoils at two axial locations ($z/R = 0.112$ and 0.4). Near the vessel base ($z/R = 0.4$), the impeller with 30° blade pitch and straight blades (HF30W25-3) attain its maximum radial velocity at $r/R = 0.36$ and $z = 0.4$ (Fig. 8A). However, a very similar trend is observed for the other impeller with the same blade shape, which has straight blades but with lesser D/T ratio (HF45W25-3). The blade width near the hub has been maintained a constant of 25 mm for all the impellers used in this work. The impeller with blade twist of 45° (HF4500W2517-3) attains a minimum radial velocity at $z/R = 0.4$ (Fig. 8A). The impellers with both blade twist and progressive decrease in blade width (HF4530W2517-3, HF6030W2513-3 and HF6045W2520-3) experiences an inward radial flow near the vessel corner at $z/R = 0.4$ and $r/R \geq 0.65$. This represents the presence of a circulation loop at the bottom which is an undesired characteristic for solid suspension operation. However, the impeller with 60° blade pitch near the impeller hub attains a maximum radial velocity of $0.22U_{tip}$ at $r/R = 0.5$ and $z/R = 0.4$. The CFD prediction for HF6045W2520-3 is under predicted at $0.4 \geq r/R \geq 0.6$. Below the impeller (Fig. 8B), the difference in radial velocity is not very marginal whereas HF6045W2520-3 experiences a maximum radial velocity of $0.078U_{tip}$ at $r/R = 0.22$ and $z/R = 0.112$.

Fig. 8C and D shows the comparisons of the mean axial velocity for the narrow bladed hydrofoils at two axial locations. Below the impeller ($z/R = 0.112$ and $r/R = 0.12$), HF4530W2517-3 and HF6045W2520-3 reaches a maximum axial velocity of $0.5U_{tip}$ whereas the 60° blade pitch hydrofoil of maximum change in blade width (HF6030W2513-3) has reached only $0.38U_{tip}$ at the same location (Fig. 8D). The hydrofoils with blade twist of 45° (HF4500W2517-3) attains an axial velocity of $0.48U_{tip}$ at $r/R = 0.2$ and $z/R = 0.12$. Similar trend was observed in the straight blade hydrofoils (HF30W25-3 and HF45W25-3). Finally, it can be observed that the hydrofoil with D/T ratio of 0.27, attains the maximum axial velocity at $r/R = 0.12$ and the hydrofoils greater than D/T ratio 0.27 attains the maximum axial velocity at $r/R = 0.2$ (Fig. 8D). Near the vessel base (Fig. 8C), the axial velocity is minimum for HF45W25-3 and HF6030W2513-3. This indicates the need of a hydrofoil to have optimum blade twist and reduction in blade width for attaining a maximum axial flow. The flow number calculation will indicate the efficient hydrofoil that gives a maximum axial flow. From Table 1, it can be concluded that the N_{QS} is maximum (1.42) for the 60° blade pitch hydrofoil (HF6045W2520-3). However, the primary flow is about 0.7 for both HF4500W2517-3 and HF6045W2520-3. The CFD predictions, below the impeller and near the vessel base matched well with the LDA measurements. The predicted mixing time from Table 1 shows a minimum value (2.53 s) for HF6045W2520-3, which has a secondary flow number of 1.42. The N_{QS} of HF6030W2513-3 was 0.72, hence, its mixing time was found to be higher (6.38 s) than other hydrofoils.

Fig. 9A and B shows the comparisons of the mean tangential velocity for the narrow bladed hydrofoils at two axial locations. The hydrofoils with 15° blade twist (HF6045W2520-3, HF4530W2517-3) experience a tangential flow in the opposite direction at $0.4 \leq r/R \leq 0.6$. Below the impeller ($z/R = 0.12$) and near the vessel base ($z/r = 0.4$), HF6045W2520-3 attains the maximum tangential velocity in the vessel centre region ($r/R < 0.15$). However away from the vessel centre, the swirling component reduces drastically for HF6045W2520-3. There is no much change in the tangential velocity trend below the impeller for other hydrofoils. The swirling component was found to be dominating in the range $0.1–0.2U_{tip}$ at $r/R = 0.4$.

Fig. 9C and D shows the comparisons of turbulent kinetic energy for the narrow bladed hydrofoils at two axial locations. Below the impeller (Fig. 9D), $z/R = 0.12$, HF4530W2517-3 attains a maximum turbulent kinetic energy of $0.046U_{tip}^2$. The power number measurement also shows a highest value ($N_P = 0.41$) for HF4530W2517-3. The hydrofoil with straight

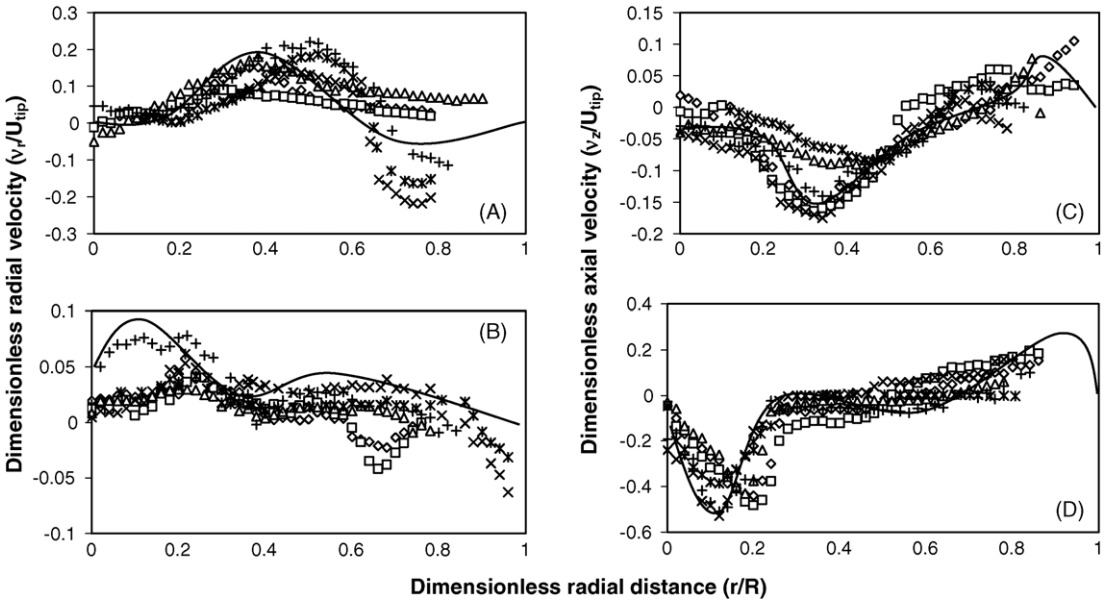

Fig. 8. Mean radial and axial velocities generated by narrow blade hydrofoils. (A and C) Near the vessel base; (B and D) below impeller; (◊) HF4; (□) HF4500W2517-3; (△) HF45W25-3; (×) HF4530W2517-3; (✱) HF6030W2513-3; (+) HF6045W2520-3; (—) CFD-HF6045W2520-3.

blades (HF30W25-3 and HF45W25-3) and with maximum blade twist (HF4500W2517-3) attains it maximum of around $0.04U_{tip}^2$ at $z/R = 0.12$ and $0.2<r/R<0.4$ whereas the 60° blade pitch hydrofoils (HF6030W2513-3 and HF6045W2520-3) attained maximum of $0.041U_{tip}^2$ at $z/R = 0.12$ and $r/R = 0.06$. The minimum power number ($N_P = 0.27$) is for the 30° pitched blade hydrofoil. Near the vessel base (Fig. 9C), the maximum value of turbulent kinetic energy is shifted in between $0.4 \leq r/R \leq 0.6$ ($z/R = 0.4$). Among all the narrow bladed hydrofoils experimented, the predicted maximum energy dissipation (118.017 m^2/s^3) was found to be maximum for HF6045W2520-3 (Table 2).

3.2.1.1. Effect of blade twist

Compared on the basis of equal power consumption (1 kW/m^3), the hydrofoil with optimum blade twist of 15° (HF6045W2520-3) gives the maximum flow number ($N_{QS} = 1.42$). However, the hydrofoil with increased blade twist (>15°) failed to pump the fluid efficiently (HF6030W2513-3). From Table 2, it can be observed that the N_{QS}/N_{QP} is maximum (2.02) for the 60° narrow blade hydrofoil that has 15° blade twist (HF6045W2520-3). If the blade twist is increased to 30°, the N_{QS}/N_{QP} drastically decrease (1.24), as in the case of HF6030W2513-3. The volume averaged normal stress was

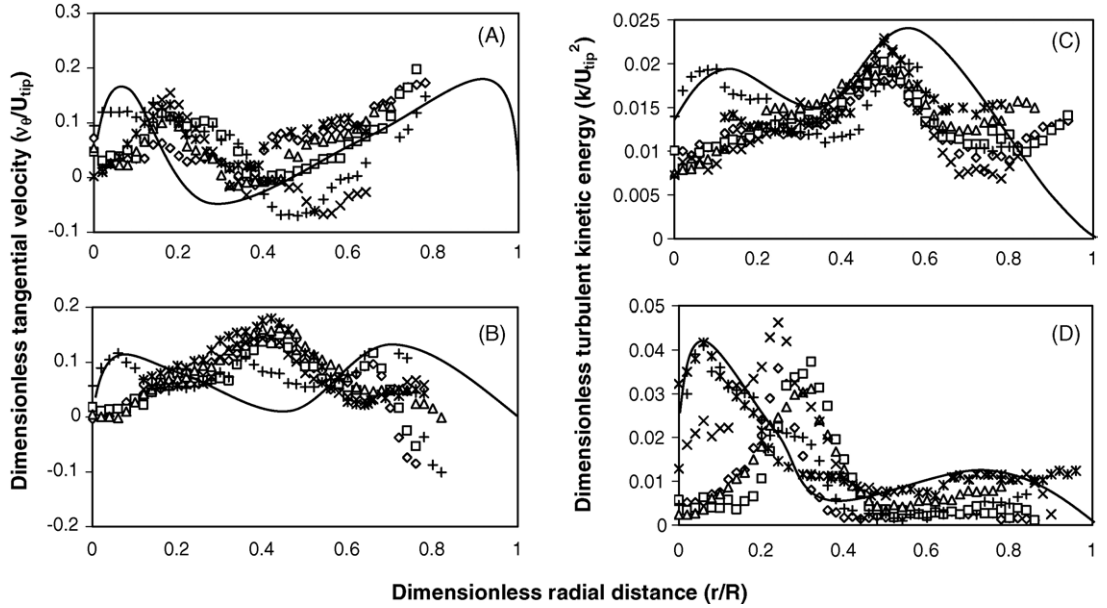

Fig. 9. Mean tangential velocity and turbulent kinetic energy flow pattern by narrow blade hydrofoils. (A and C) Near the vessel base; (B and D) below impeller; (◊) HF4; (□) HF4500W2517-3; (△) HF45W25-3; (×) HF4530W2517-3; (✱) HF6030W2513-3; (+) HF6045W2520-3; (—) CFD-HF6045W2520-3.

found to be higher (10.08 N/m^2) for HF4530W2517-3. Similarly the shear rate is found to be higher (1.032 s^{-1}) for HF4530W2517-3. The average turbulent kinetic energy is found to be about 0.015 m^2/s^2, which is well reflected in the torque measurements (N_P = 0.41) for HF4530W2517-3.

3.2.1.2. Effect of blade width

The hydrofoil with constant blade width (HF30W25-3 and HF30W25-3) gives the minimum N_{QP} of 0.57. Hydrofoils with decreasing blade width increase the N_{QP}.

3.3. Broad bladed hydrofoils

The use of high-solidity, axial flow down-pumping impellers in fermenters have resulted in a wide variety of both positive and negative results. Much of this may come from the complexity of the biological process on fermentations. Such impeller designs are also utilised in the mixing of slurry, pulp and paper industries, etc. However, the overall turbulence level has to be investigated especially when papillation in bio-reactors is found be a major factor for the death rate [24]. In the present study, four broad bladed hydrofoils with two W/D ratios (0.5 and 0.8) were taken for the experimentation.

Fig. 10A and B shows the comparison of the mean radial velocity for broad bladed hydrofoils at two axial locations. Near the vessel base (z/R = 0.4), the trend for all the four broad bladed hydrofoils are similar. The maximum radial velocity attained by the four-bladed hydrofoil (HF3) is $0.128U_{tip}$ and that of three-bladed hydrofoil (HF2) is $0.122U_{tip}$ at r/R = 0.24. Similarly for hydrofoils with the change in the blade width (HF3045-4 and HF4560-4), the maximum radial velocity is $0.096U_{tip}$ and $0.089U_{tip}$ respectively at z/R = 0.2 and r/R = 0.2. Below the impeller (z/R = 0.18), there is no much difference in the radial velocity trend for HF2 and HF3. The radial flow near the baffle region is very similar for all the four broad bladed hydrofoils at z/R = 0.4. For brevity the profiles above the impeller and near the vessel surface are not given.

Fig. 10C and D shows the comparison of the mean axial velocity for broad bladed hydrofoils at two axial locations. The axial jet below the impeller (z/R = 0.18) for the four-bladed hydrofoil (HF3) can reach up to $0.68U_{tip}$ at r/R = 0.26, whereas the three-bladed hydrofoil of the same blade design attains $0.52U_{tip}$ at r/R = 0.22 (Fig. 10D). The measured flow number below the impeller represents that the hydrofoil with four blades (HF3) are energy efficient impellers (N_{QS} = 2.44). Table 1 shows a good improvement in both the primary and secondary flow numbers. The N_{QP} and N_{QS} of HF3 increased to about 3% and 10% when compared with HF2, respectively. The primary flow number is 0.7 for both HF3045-4 and HF4560-4. Almost 50% of the primary flow is reduced when compared with HF3. Near the vessel base (z/R = 0.4), the trend for the axial velocity profile is similar as below the impeller (Fig. 10C). The downward jet strength is almost diminished (HF3045-4 and HF4560-4) to 50% near the vessel base where it is converted to radial flow. The mixing time was found to be minimum (θ_{CFD} = 4.63 s) for HF3 hydrofoil and maximum (θ_{CFD} = 6.53 s) for HF4560-4.

Fig. 11A and B shows the comparison of the mean tangential velocity for the broad bladed hydrofoils at two axial locations. There is negligible difference in the tangential profile of HF2 and HF3 near the vessel base at z/R = 0.4 (Fig. 11A). A strong vortex is seen for both HF2 and HF3 in the vessel core region (r/R< 0.3) at z/R = 0.4 whereas the swirling component for hydrofoil with change in blade width (HF3045-4 and HF4560-4) is almost 50% lesser than HF2/HF3. A very similar trend is observed below the impeller (z/R = 0.18), in the vessel core region (Fig. 11B). The tangential velocity for HF2/HF3 is almost 40% higher than that of HF3045-4/HF4560-4 at $r/R \leq 0.4$.

Fig. 11C and D shows the comparisons of turbulent kinetic energy for the broad bladed hydrofoils at two axial locations. Below the impeller, at z/R = 0.18 and r/R = 0.34, HF3 attains a maximum turbulent kinetic energy of $0.0414U_{tip}^2$. The torque measurements also show higher value for HF3 (N_P = 3.34). The four-bladed hydrofoil (HF3) attains a maximum local turbulent kinetic energy away from the baffle region. It is also found that the maximum kinetic energy is due to the axial fluctuations. It is clear that the axial pumping improves at the expense of axial fluctuations for HF2 and HF3. As the number of blade reduces from four (HF3) to three (HF2), power number reduced by 30% (N_P = 2.32). The power number is less for both HF3045-4 and HF4560-4. However, HF3045-4 and HF4560-4 was found to be poor in axial pumping. The predicted maximum energy dissipation rate was found to be higher (12.915 m^2/s^3) for HF4560-4. The predicted maximum energy dissipation rate for HF3 was found to be 10.236 m^2/s^3, which was in good agreement with the work of Ghadge et al. [25], where they used cellulase enzyme solution as working fluid. The average turbulent normal stress ($\overline{\tau}_N$) is dominated by the axial fluctuation that was found to be 28.66 N/m^2 for HF3. Similarly the average shear rate is 8.383 s^{-1} for HF3. Please note that the CFD predictions and comparisons have been presented for only one of the cases for the sake of clarity.

3.4. Radial flow impeller

The disc turbine is most extensively studied impeller in the literature. The flow in the discharge stream of Rushton turbine is characterized by the existence of strong radial and tangential components of mean velocity, periodic and fluctuating component. The details of the vortex pair generated behind the impeller blade are dealt in detail by Yianneskis et al. [26], Zhou and Kresta [15], Hockey and Nouri [21], Kemoun et al. [27] and Renaud et al. [28]. It is also emphasized that the vortex trajectory is dependent on the impeller diameter. For the completeness of the work, a standard disc turbine (D/T = 0.33; C/T = 0.33; T = 500 mm) was used to predict the turbulent kinetic energy. The average value of primary pumping number is around 0.75. The maximum axial velocities in the bulk of the tank are of the order of $0.2U_{tip}$. Radial velocities are predominant at the top and bottom of the vessel that are in the order of $0.1–0.2U_{tip}$. Turbulence characteristics in the impeller stream of disc turbine have been studied by many investigators [29,26,30,31,15,27,32]. Ng et al. [33,34] have used

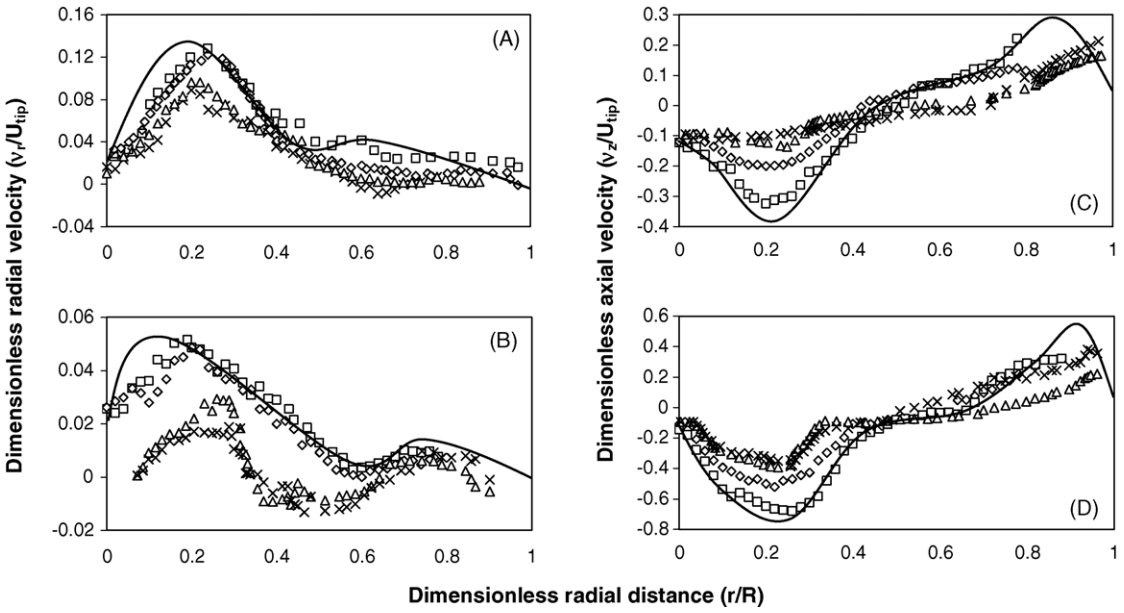

Fig. 10. Mean radial and axial velocities generated by broad blade hydrofoils. (A and C) Near the vessel base; (B and D) below impeller; (◊) HF2; (□) HF3; (△) HF3045-4; (×) HF4560-4; (—) CFD-HF3.

sliding mesh approach and investigated the effect of grids in the range 46,016–239,468. They have shown that the predictions of RANS based models do not agree with the experimental data obtained in the impeller discharge line of the experimental data. Wechsler et al. [35] have used 400,000 and 1,000,000 grids and still the predictions deviated by 50%. In this work, we have used similar approach with the improvements that the LDA data has been deionised using multiresolution analysis which employs wavelet transforms [17]. We have used 443,800 grids for the simulation. Figs. 12 and 13 show the comparison between the CFD predictions and the experimental data (T = 500 mm, D/T = 0.33, C/T = 0.33) near the impeller zone and in the bulk region, respectively.

4. Relation between the impeller design and gross flow characteristics

In the present work, a large number of impellers were fabricated and investigated in terms of its hydraulic efficiencies (N_{QP}/N_P and N_{QS}/N_P). The primary hydraulic efficiency (N_{QP}/N_P) varied from 0.39 to 2.37, whereas the secondary hydraulic efficiency (N_{QS}/N_P) was found in the range 0.47–4.53.

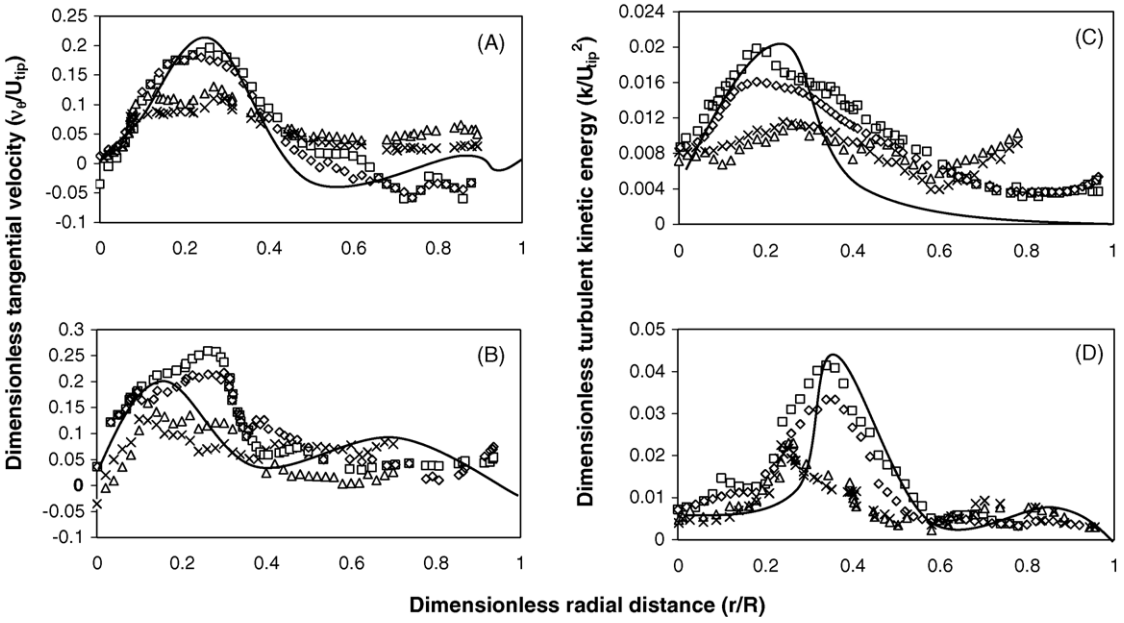

Fig. 11. Mean tangential velocity and turbulent kinetic energy flow pattern by broad blade hydrofoils. (A and C) Near the vessel base; (B and D) below impeller; (◊) HF2; (□) HF3; (△) HF3045-4; (×) HF4560-4; (—) CFD-HF3.

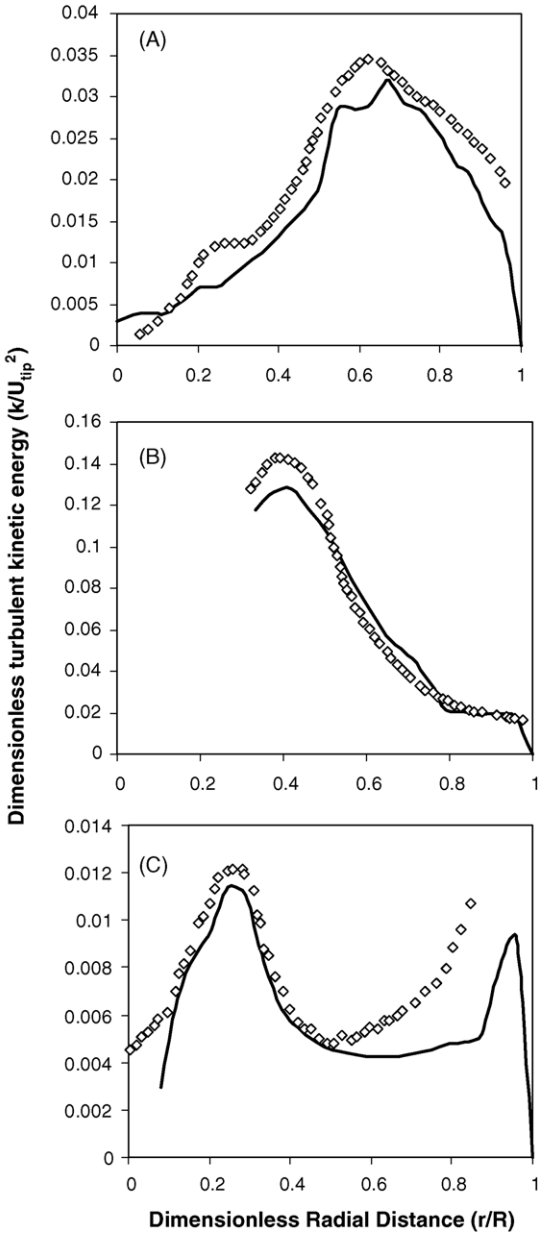

Fig. 12. Turbulent kinetic energy flow pattern by radial flow turbine: (A) 30 mm below the impeller plane; (B) in the impeller plane; (C) 30 mm above the impeller plane. (◊) LDA measurement; (—) CFD prediction.

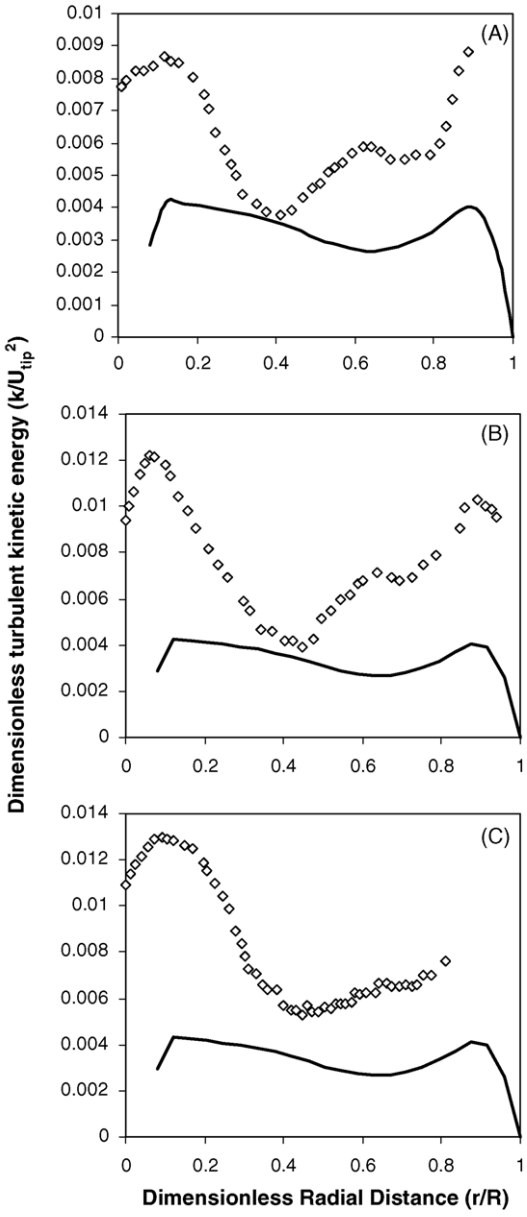

Fig. 13. Turbulent kinetic energy flow pattern by radial flow turbine: (A) 50 mm above the impeller plane; (B) 65 mm above the impeller plane; (C) 80 mm above the impeller plane. (◊) LDA measurement; (—) CFD prediction.

However, the narrow blade hydrofoil, HF6045W2520-3, was found to give maximum hydraulic efficiency ($N_{QP}/N_P = 2.37$ and $N_{QS}/N_P = 4.53$). The ratio of ε_{max}/N^3D^2 was found to be minimum for the narrow blade hydrofoil HF6045W2520-3 (0.869) and maximum for PBTD60W3085-6 (5.218). However, the difference in ε_{max}/N^3D^2 for HF6045W2520-3 (0.869) and HF6030W2513-3 (0.897) was found to be only 3%. The values of k_{avg} are the indicative of turbulence generated by an impeller, whereas N_{QS} indicates the total axial mean flow generated by an impeller. The results indicate that the optimized mixing time for narrow blade hydrofoil was found with the HF6045W2520-3 until the average turbulent kinetic energy (k_{avg}) level is 8% of the standard pitched blade turbine used by Patwardhan and Joshi [1], which is kept as the base case. Further, it can also be observed at equal power consumption level of 1 W/kg, the broad blade hydrofoil HF3 gave minimum dimensionless mixing time of 59.18 with $N_{QP}/N_P = 0.455$ and $N_{QS}/N_P = 0.745$. The average normal stress ($\bar{\tau}_N$) was found to be maximum (81.4 N/m^2) for PBTD60W50-6 and minimum (6.57 N/m^2) for HF30W25-3. The average shear rate (γ_{avg}) was maximum (8.383 s^{-1}) for broad blade hydrofoil, HF3 and minimum (0.673 s^{-1}) for narrow blade hydrofoil, HF30W25-3. Of all the impellers used in the present study, broad blade hydrofoils and 60° PBTD generates maximum level of shear ($\gamma_{avg} > 4$ s^{-1}). However, the 30° PBTD generates a medium level of shear ($\gamma_{avg} = 1.5$–2 s^{-1}). Hence, HF3 impeller may be more suitable for dispersion applications whereas the narrow blade hydrofoils are more suitable for blending application and shear sensitive products.

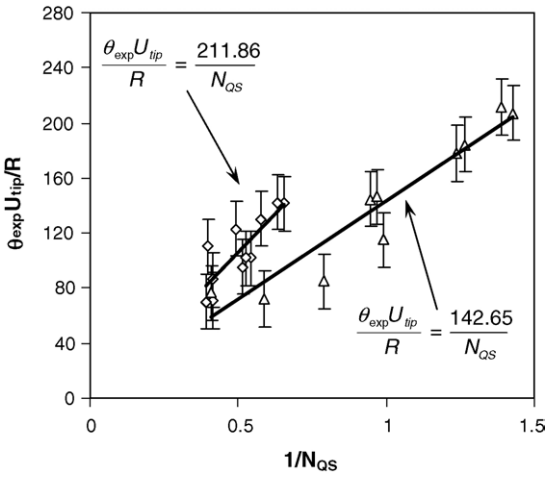

Fig. 14. Relation between dimensionless mixing time ($\theta_{exp}U_{tip}$/R) and $1/N_{QS}$; (◊) PBTD; (△) hydrofoils.

5. Relation between the impeller design and mixing time

The effect of impeller design, blade pitch, blade width and blade twist were investigated on the mean and turbulence characteristics as well as mixing time. The results are given in Table 2. In all the cases, the mixing time was found to be inversely proportional to the secondary flow number (N_{QS}) of an impeller, irrespective of the nature of impeller design. Patwardhan and Joshi [36] have found that the mixing time for axial flow impellers could be correlated well with the secondary flow number (N_{QS}). Similar relationship was found to hold for all the impellers. However, an interesting observation was made. A plot of dimensionless mixing time ($\theta_{exp}U_{tip}/R$) versus flow number showed two distinct times. One corresponding to pitched blade turbines (impellers 1–12 in Table 1) and hydrofoils (impellers 13–22 in Table 1). These times are shown in Fig. 14 and given by the following equations. The proportionality constant can be seen to be 211.86 for pitched blade turbines and 142.65 for hydrofoils. The proportionality constant for hydrofoils is almost 1.5 times lower than PBTD

$$\frac{\theta_{exp}U_{tip}}{R} = \frac{211.86}{N_{QS}} \quad (11)$$

$$\frac{\theta_{exp}U_{tip}}{R} = \frac{142.65}{N_{QS}} \quad (12)$$

The maximum and minimum error deviation for the line with proportionality constant 211.86 (PBTD) was found to be 24% and 4%, respectively (Fig. 14). On an average, the ordinate error deviation was found to be 15%. Similarly, the maximum and minimum error deviation for the line with proportionality constant 142.65 (hydrofoils) was found to be 30% and 4%, respectively. On an average, the ordinate error deviation was found to be 19%.

6. Conclusion

In the present work, a combination of LDA measurements and CFD predictions using sliding mesh approach has been performed to study the effect of impeller design on the flow pattern (average velocity, turbulent kinetic energy, maximum energy dissipation rate, average shear rate and turbulent normal stress) and mixing time for a set of axial flow impellers (pitched blade turbines and hydrofoils). A very good agreement has been observed between experimental and the predicted mixing time over a wide range of impellers varying in number of blades, blade angle, blade width and impeller diameter. When compared at an equal power consumption level of 1 kW/m^3, the following conclusions can be drawn regarding the effects of different impeller design parameters.

(1) As the impeller angle increases from 30° to 60°, the N_{QS}/N_{QP} ratio was found to be 2.15 and 2.17 for 30° and 45° pitch, respectively, whereas it reduced to 1.73 for 60° pitched blade impeller. Similarly, the N_{QS}/N_P ratio was also found to decrease with an increase in the blade angle [30° (2.4); 45° (1.01); 60° (0.72)].

(2) Power number and the secondary flow number were found to decrease with a decrease in W/D ratio. (PBTD45W30-6 ($N_P = 1.41$; $N_{QS} = 1.85$), PBTD45W50-6 ($N_P = 1.8$; $N_{QS} = 2.02$)). The N_{QS}/N_P ratio was also found to decrease with a decrease in W/D ratio.

(3) It was observed that the presence of blade twist (PBTD3020W50-6) decreases the power number and flow numbers.

(4) For a downflow impeller, the jet leaving the impeller interacts with the vessel base, producing more energy dissipation (PBTD45W30-6; $\varepsilon_{max}/N^3D^2 = 2.53$) in the region below the impeller. For an upflow impeller, the jet leaving the impeller interacts with the top liquid surface, where the energy dissipation was found to be comparatively smaller (PBTU45W30-6; $\varepsilon_{max}/N^3D^2 = 2.24$). The average shear rate, average normal stress and turbulent kinetic energy were found to be higher for the downflow impellers.

(5) The narrow blade hydrofoil impeller with a blade twist of 15° (HF6045W2520-3) gives the maximum flow number ($N_{QS} = 1.42$). Further increase in blade twist (>15°) resulted into a decrease in flow number. The narrow blade hydrofoil without blade twist (HF30W25-3 and HF30W25-3) gives low flow number ($N_{QP} = 0.57$).

(6) In the present work, four designs of four-bladed impellers (PBTD45W50-4, HF3, HF3045-4, HF4560-4) have been investigated. Out of these, HF3 design was found to give highest values of N_{QP} and N_{QS} followed by conventional four-bladed pitched blade turbine (PBTD45W50-4 (Fig. 1F)). The other two hydrofoil designs (HF3045-4 and HF4560-4) have relatively very low flow numbers.

(7) It was observed that the dimensionless mixing time ($\theta_{exp}U_{tip}/R$) varies inversely with the secondary flow number (N_{QS}) of the impeller. The proportionality constant can be seen to be 211.86 for pitched blade turbines and 142.65 for hydrofoils. The proportionality constant for hydrofoils is almost 1.5 times lower than PBTD.

Acknowledgements

This work has been part of the project program supported by Board of Research in Nuclear Sciences (BRNS), Sanction No. 2002/34/7-BRNS/140. Kumaresan acknowledges the fellowship support given by the University Grants Commission (UGC), Government of India.

References

[1] A.W. Patwardhan, J.B. Joshi, Relation between flow pattern and blending in stirred tanks, Ind. Eng. Chem. Res. 38 (1999) 3131–3143.
[2] R.K. Firoz, D.R. Chris, K.H. Grahan, A multi-block approach to obtain angle resolved PIV measurements of the mean flow and turbulence fields in a stirred vessel, Chem. Eng. Technol. 27 (2004) 264–269.
[3] M. Schafer, M. Yianneskis, P. Wachter, F. Durst, Trailing vortices around a 45° pitched blade impeller, AIChE J. 44 (1998) 1233–1265.
[4] J.B. Fasano, A. Bakker, W.R. Penney, Advanced impeller geometry boosts liquid agitation, Chem. Eng. (1994) 110–116.
[5] V.V. Ranade, J.B. Joshi, Flow generated by pitched blade turbines. I. Measurements using laser Doppler anemometer, Chem. Eng. Commun. 81 (1989) 197–224.
[6] L. We-Ming, W. Hong-Zhang, C. Nai-Yu, L. Yu-Li, Effect of the blade size on the vortex structure and gas dispersion in gas–liquid stirred vessels with a single Rushton turbine impeller, Proc. Natl. Sci. Counc. ROC(A) (2000) 166–175.
[7] K. Rutherford, M.S. Mahmoudi, K.C. Lee, M. Yianneskis, The influence of Rushton impeller blade and disk thickness on the mixing characteristics of stirred vessels, Chem. Eng. Res. Des. 74 (1996) 369–378.
[8] W. Bujalski, A.W. Nienow, S. Chatwin, M. Cooke, The dependency on scale of power numbers of Rushton disc turbines, in: Proceedings of the International Conference on Mechanical agitation, Toulouse, 1986, pp. 1.37–1.46.
[9] J. Medek, I. Fort, Mixing in vessel with eccentrical mixer, in: Proceedings of the Fifth European Conference on Mixing, Wurzburg, Germany, 1985, pp. 263–271.
[10] N.J. Fentiman, N.S.T. Hill, K.C. Lee, G.R. Paul, M. Yianneskis, A novel profiled blade impeller for homogenization of miscible liquids in stirred vessels, Chem. Eng. Res. Des., Part A 76 (1998) 835–842.
[11] Z. Jaworski, A.W. Nienow, K.N. Dyster, An LDA study of the turbulent flow field in a baffled vessel agitated by an axial, down-pumping hydrofoil impeller, Can. J. Chem. Eng. 74 (1996) 3–15.
[12] M. Tomas, V. Linek, P. Eva, Gas hold-up, mixing time and gas–liquid volumetric mass transfer coefficient of various multiple-impeller configurations: Rushton turbine, pitched blade and techmix impeller and their combinations, Chem. Eng. Sci. 58 (2003) 1839–1846.
[13] S. Bugay, E. Renaud, L. Alain, Experimental analysis of hydrodynamics in axially agitated tank, AIChE J. 48 (2002) 463–475.
[14] P. Mavros, C. Xuereb, J. Bertrand, Determination of 3-D flow fields in agitated vessels by laser Doppler velocimetry: use and interpretation of RMS velocities, Chem. Eng. Res. Des. 76 (1998) 223–233.
[15] G. Zhou, S.M. Kresta, Distribution of energy between convective and turbulent flow for three frequently used impellers, Chem. Eng. Res. Des. 74 (1996) 379–389.
[16] S.P. Swapnil, A.D. Niteen, J.B. Joshi, Mass transfer characteristics of surface aerators and gas inducing impellers, Ind. Eng. Chem. Res. 43 (2004) 2765–2774.
[17] A.A. Kulkarni, J.B. Joshi, V. Ravi Kumar, B.D. Kulkarni, Application of multiresolution analysis for simultaneous measurement of gas and liquid velocities and fractional hold-up in bubble column using LDA, Chem. Eng. Sci. 56 (2001) 5037–5048.
[18] A. Sahu, P. Kumar, J.B. Joshi, Simulation of flow in stirred vessel with axial flow impeller: zonal modeling and optimization of parameters, Ind. Eng. Chem. Res. 37 (1998) 2116–2130.
[19] R.B. Bird, W.E. Stewart, E.N. Lightfoot, Transport Phenomena, John Wiley & Sons, Inc., New York, 1994.
[20] V.V. Ranade, V.P. Mishra, G.B. Saraph, G.B. Deshpande, J.B. Joshi, Comparison of axial flow impellers using a laser Doppler anemometer, Ind. Eng. Chem. Res. 31 (1992) 2370–2379.
[21] R.M. Hockey, J.M. Nouri, Turbulent flow in a baffled vessel stirred by a 60° pitched blade impeller, Chem. Eng. Sci. 51 (1996) 4405–4421.
[22] S. Kresta, P. Wood, The mean flow field produced by a pitched blade turbine: changes in the circulation pattern due to off bottom clearance, Can. J. Chem. Eng. 71 (1993) 42–53.
[23] C. Galletti, A. Paglianti, K.C. Lee, M. Yianneskis, Reynolds number and impeller diameter effects on instabilities in stirred vessels, AIChE J. 50 (2004) 2050–2063.
[24] H.M. Sudhanshu, K. Niranjan, Observations on the shear damage to different animal cells in a concentric cylinder viscometer, Biotech. Bioeng. 68 (6) (2000) 697–704.
[25] R.S. Ghadge, A.W. Patwardhan, S.B. Sawant, J.B. Joshi, Effect of flow pattern on cellulase deactivation in stirred tank bioreactors, Chem. Eng. Sci. 60 (2005) 1067–1083.
[26] M. Yianneskis, Z. Popiolek, J.H. Whitelaw, An experimental study of the steady and unsteady flow characteristics of stirred reactors, J. Fluid Mech. 175 (1987) 537–555.
[27] A. Kemoun, F. Lusseyran, M. Mahouast, J. Mallet, Experimental determination of the complete Reynolds stress tensor in fluid agitated by a Rushton turbine, in: Proceedings of the Eighth European Conference on Mixing, 1994, pp. 399–406.
[28] E. Renaud, B. Denis, L. Alain, Characterization of trailing vortices generated by a Rushton turbine, AIChE J. 50 (2004) 75–86.
[29] J. Drbohlav, I. Fort, K. Maca, J. Placek, Turbulent characteristics of discharge flow from the turbine impeller, Coll. Czech. Chem. Commun. 43 (1978) 3148–3162.
[30] J. Costes, J.P. Couderc, Study by laser Doppler anemometry of the turbulent flow induced by a Rushton turbine in a stirred tank: influence of the size of the units. I. Mean flow and turbulence, Chem. Eng. Sci. 43 (1988) 2751–2764.
[31] V.V. Ranade, J.B. Joshi, Flow generated by a disc turbine. I. Experimental, Chem. Eng. Res. Des. 81 (1990) 197–224.
[32] K.C. Lee, M. Yianneskis, Turbulence properties of the impeller stream of a Rushton turbine, AIChE J. 44 (1998) 13–24.
[33] K. Ng, M. Yianneskis, Assessment of sliding mesh CFD predictions and LDA measurements of the flow in a tank stirred by a Rushton impeller, Chem. Eng. Res. Des. 76 (1998) 737–747.
[34] K. Ng, M. Yianneskis, Observations on the distribution of energy dissipation in stirred vessels, Chem. Eng. Res. Des. 78 (2000) 334–341.
[35] K. Wechsler, M. Breuer, F. Durst, Steady and unsteady computations of turbulent flows induced by a 4/45° pitched blade impeller, J. Fluids Eng. 121 (1999) 318–329.
[36] A.W. Patwardhan, J.B. Joshi, CFD—an emerging tool for the design of stirred vessel, in: Proceedings of Third International Symposium on Mixing in Industrial Processes, 1999, pp. 13–20.